Spring 2018

Crustal Structure of the Bhutanese Himalaya: New Insights from a Gravity Analysis in Western and Central Bhutan

Kinzang Duba
Missouri State University, kinzangduba705@gmail.com

CRUSTAL STRUCTURE OF THE BHUTANESE HIMALAYA: NEW INSIGHTS FROM A GRAVTITY ANALYSIS IN WESTERN AND CENTRAL BHUTAN

A Master's Thesis

Presented to

The Graduate College of

Missouri State University

In Partial Fulfillment

Of the Requirements for the Degree

Master of Science, Geospatial Science in Geography, Geology and Planning

By

Kinzang Duba

May 2018

CRUSTAL STRUCTURE OF THE BHUTANESE HIMALAYA: NEW INSIGHTS FROM A GRAVTITY ANALYSIS IN WESTERN AND CENTRAL BHUTAN

Geography, Geology and Planning

Missouri State University, May 2018

Master of Science

Kinzang Duba

ABSTRACT

To expand the current understanding of lithospheric structure within Bhutan Himalaya, a detailed gravity survey was conducted for the first time along the all major roads within western and central Bhutan in 2015-2017. The acquired Bouguer gravity anomaly data were analyzed and interpreted using map methods (wavelength filtering and Euler deconvolution) which clearly indicate that there are substantial anomalies due to crustal density sources and a complex Himalayan geology. Four two-dimensional gravity models across the Himalayan tectonostratigraphic units were constructed to determine the crustal density structure using constraints from the geological and geophysical studies. The results support that the long wavelength gravity anomalies are associated with variations of the Moho depth that are caused by the flexure of Indian plate. The modelling revealed along-strike differences in the crustal thickness beneath Bhutan Himalaya. In western Bhutan, the Moho depth increases towards the north from ~50 km beneath the Main Frontal Thrust to ~70 km beneath the Greater Himalaya, whereas in central Bhutan the Moho was imaged at depth varying between ~50 and ~60 km. The Bhutan Himalayan orogenic wedge is detached from the underlying Indian plate along the basal decollement known as the Main Himalayan Thrust at a depth increasing from 7-10 km beneath Sub and Lesser Himalaya to ~30 km beneath the Greater Himalaya.

KEYWORDS: Bhutan Himalaya, Bouguer gravity anomaly, crustal structure, gravity modeling.

This abstract is approved as to form and content

_____

Kevin L. Mickus, DGS
Chairperson, Advisory Committee
Missouri State University

CRUSTAL STRUCTURE OF THE BHUTANESE HIMALAYA: NEW INSIGHTS FROM A GRAVTITY ANALYSIS IN WESTERN AND CENTRAL BHUTAN

By

Kinzang Duba

A Master's Thesis
Submitted to the Graduate College
Of Missouri State University
In Partial Fulfillment of the Requirements
For the Degree of Master of Science, Geospatial Science
in Geography and Geology

May 2018

Approved:

_____
Kevin L. Mickus, DGS

_____
Melida Gutiérrez, PhD

_____
Matthew P. McKay, PhD

_____
Julie Masterson, PhD: Dean, Graduate College

ACKNOWLEDGEMENTS

I would like to acknowledge and thank my committee members, Dr. Kevin Lee Mickus, Dr. Melida Gutierrez, and Dr. Matthew P. McKay for their support and guidance. I remain deeply indebted to my supervisor Dr. Kevin Lee Mickus, who not only accepted me as his research student, but also have been instrumental for the completion of this project with his valuable guidance, intellectual support and encouragements during the entire period and beyond the academic breadth.

I acknowledge Mr. Brain Gosling from National Geospatial and Imaging Agency (NGA) for the financial support and Mr. Mike Prugger for shipping of equipment from NGA to Bhutan. Our field work would not have been possible without the assistance from my employer the Department of Geology and Mines (DGM) and particularly Mr. Ugyen Wangda, Chief Geologist for his full cooperation and unwavering support. My sincere appreciation to Mr. Kinzang Thinley and Mr. Tenzin Norbu from the National Land Commission Secretariat for providing GPS data for PRS station.

Sincerely thanking Dr. Tobgay for introducing me to Dr. Mickus and providing extremely useful feedbacks, Mr. Matthew Zerilli and his family, and colleagues from DGM. Finally, I share this achievement with my parents, wife and son whose enduring blessing, love and support made this endeavor a pleasant journey.

TABLE OF CONTENTS

LIST OF TABLES

LIST OF FIGURES

1. INTRODUCTION

The Himalayan orogeny is the result of collision between the Indian and Eurasian plates that initiated during the Eocene period (Le Fort, 1975; Gansser, 1983; Molnar, 1986; Hodges, 2000). As one of the youngest orogenic features on Earth, the Himalaya orogenic belt is an active tectonic regime, with the Indian subcontinent moving towards the Eurasian continent at an average rate of 55 mm/yr with respect to the Eurasia plate at the present day (Searle, 2013). This Cenozoic orogenesis deformed sedimentary suites along the northern margin of the Indian craton deposited from early Proterozoic through Pliocene time (McQuarrie et al., 2008) by stacking thrust along the major foreland directed thrust faults that link with a supra-regional basal decollement known as the Main Himalayan Thrust (Zhao et al., 1993; Grujic et al., 1996; Hauck et al., 1998).

In the Himalayan orogeny, deformation is manifest through a combination of frontal accretion in the upper crust, underthrusting of the Indian plate and the formation of an upper crustal fold-thrust belt (Avouac, 2003, 2007; Singer et al., 2017a). Therefore, the subsurface structure holds an important information concerning the crustal evolution during the collisional orogenesis. Numerous geophysical investigation including seismic and gravity studies have been conducted across the Himalayan orogenic belt in order to resolved the lithospheric structures that enhances the understanding of the ongoing orogenic evolution (Lyon-Caen and Molar, 1985; Zhao et al., 1993; Hauck et al., 1998; Tiwari et al., 2006; Wittlinger et al., 2009; Nábělek et al., 2009; Acton et al., 2011; Chamoli et al., 2010; Bai et al., 2013; Ansari et al., 2014). Results from all these studies have revealed 1) thickened crust beneath Greater Himalaya and Southern Tibet from the

flexure of the Indian plate, 2) a north dipping crust/mantle boundary with abrupt increase in dip angles beneath the Greater Himalayan, and 3) the geometry of crustal structures like the Main Himalayan Thrust with a ramp beneath the Greater Himalayan. The majority of these studies, however, were focused on the Indian and Nepalese Himalayan part of the orogenic belt leaving the Bhutan Himalaya in the eastern quarter of the Himalayan orogeny (Fig. 1), poorly constrained using geophysical studies.

A detailed geophysical data analysis beneath Bhutan Himalaya may provide unprecedented insight regarding the evolution of Himalayan orogen. As of now, the surface-based studies have inferred subsurface geometries beneath Bhutan Himalaya based on balanced cross sections construction (McQuarrie et al., 2008; Long et al., 2011b; Tobgay et al., 2012). Recently, seismic and gravity investigations imaged the major lithospheric structures beneath Bhutan Himalaya, which include studies based on a seismic receiver function analysis (Singer et al., 2017a), seismic ambient noise tomography (Singer et al., 2017b), and a regional scale gravity analysis (Hammer et al., 2013). The study on the geometry of Main Himalayan Thrust using thermochronologic data (Coutand et al., 2014) includes another constraint on the geometry of the Bhutanese Himalayan orogen.

To date, subsurface models may be improved by the incorporation on a potential field analysis. This study uses new detailed gravity data acquired across the orogenic wedge of western and central Bhutan. The gravity data analyzed using a variety of map analysis methods including wavelength filter, isostatic residual gravity anomalies, and derivatives methods provide insight into the gravity measurements. The gravity data, in addition to available geologic and seismic data, form the basis for a series of two-

dimensional (2-D) gravity models to test potential lithospheric structures beneath the Bhutanese Himalaya. The final models will be interpreted in terms to determine the lithospheric structure and tectonic evolution of western and central Bhutan.

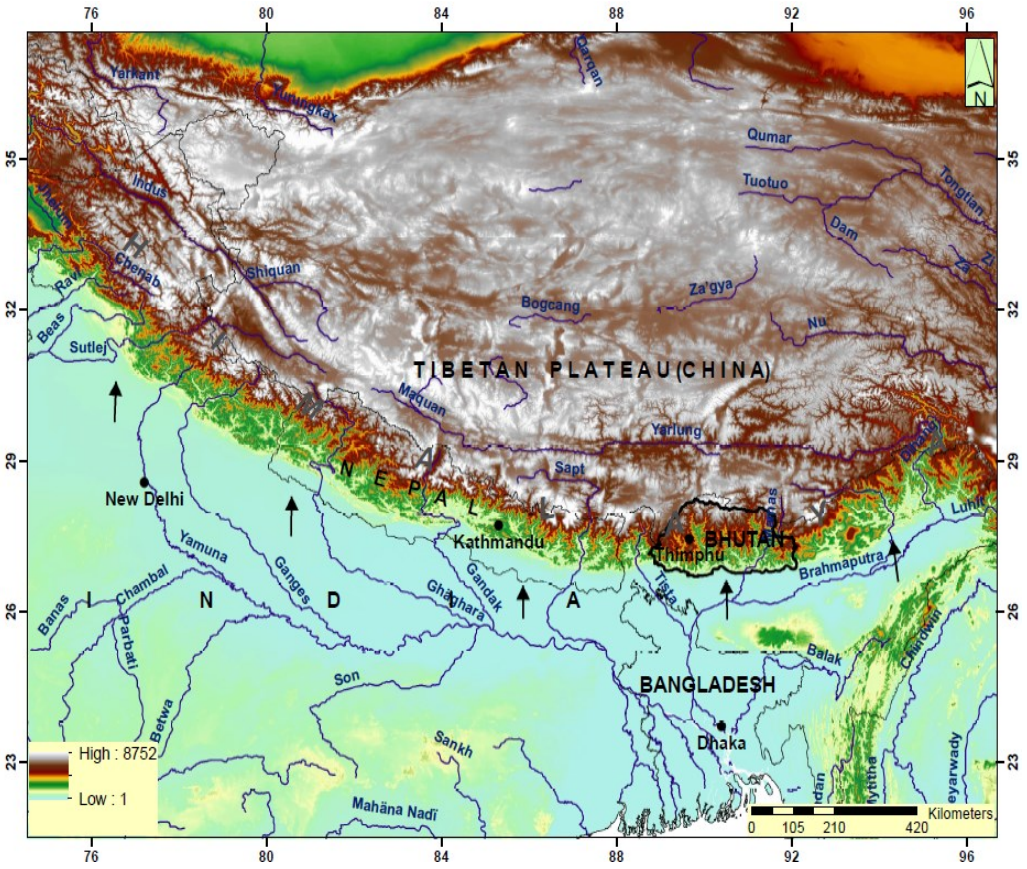

Figure 1. Geographic map of the Himalaya. The direction of arrows shows the direction of movement of Indian Plate and the study area is highlighted with dark lines.

1.1 Objective and Scope of Study

The main objective of this study is to examine and map the lithospheric structures beneath the western and central Bhutan Himalaya through the analysis of gravity data. To achieve this objective, densely spaced stations of gravity data were collected along and across the Himalayan orogenic wedge in western and central Bhutan. A total of

approximately 2300 gravity data points were processed and analyzed to produce a series of gravity maps, including Bouguer gravity anomaly, band-pass filtered, horizontal derivative, and isostatic residual gravity. These maps offer a significant insight about the general geologic nature of the study area. The extended Euler three-dimensional (3D) deconvolution method was used to proximate the boundary of tectonic structures and the depth of the source body. And to acquire a comprehensive quantitative representation of the subsurface structures, 2D forward gravity models were constructed along the specified profile within the area of interest.

2. GEOLOGY AND TECTONICS

2.1 Regional Tectonics

The Himalayan orogenic belt comprises four tectonostratigraphic sequences, each bounded by crustal-scale fault systems that span the entire length of the orogen (Heim and Gansser, 1939; Gansser, 1964, 1983; Le Fort, 1975; McQuarrie et al., 2008; Tobgay et al., 2012). From south to north, the tectonostratigraphic sequences are the Sub Himalaya , the Lesser Himalaya, the Greater Himalaya and the Tethyan Himalaya, and their bounding fault systems includes the Main Frontal thrust, the Main Boundary thrust, the Main Central thrust and the South Tibetan Detachment system (Fig. 2). A brief summary and definition of all the major litho-tectonic units and tectonic structures of Himalaya are shown in Tables 1 and 2. The tectonostratigraphic sequences of Himalayan orogeny were originally defined based on the change in metamorphic grade of the rocks in which abrupt juxtaposition of higher grade rocks over lower grade rocks. These tectonic sequences were used to define the main orogen structures including the Main Himalayan Thrust and Main Boundary Thrust (Heim and Gansser, 1939; Gansser, 1964; Le Fort, 1975; Tobgay et al., 2010). The Himalaya orogen gradually evolved as these orogeny-structures propagated southward as India collided with Eurasia.

The Tethyan Himalayan sequence records the oldest Himalayan deformation, and it sits structurally and geographically above the other stratigraphic zones (Godin et al., 2006; McQuarrie et al., 2008). The Tethyan sequence represents the weakly metamorphosed Paleozoic to Mesozoic shelf deposits that formed on the northern margin of the Indian Craton as it moved northward. It comprises two superimposed rift to passive

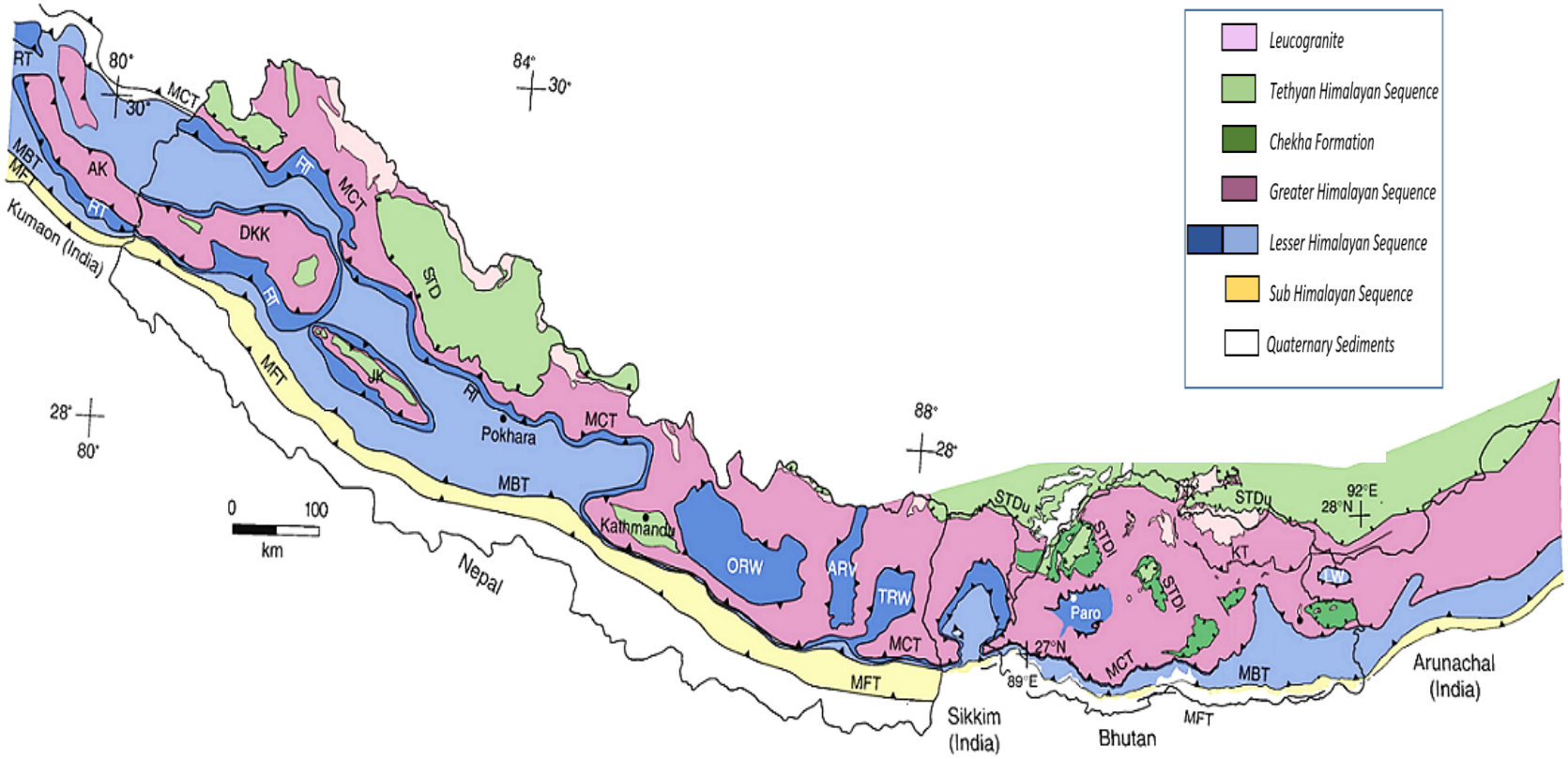

Figure 2. A simplified geological map of the Himalaya with major tectonic structures. It includes Bhutan, Nepal and part of the Indian Himalaya. AK=Almora klippe, DKK=Dadeldhura/Karnali klippe, JK=Jajarkot klippe, ORW=Okhadunga/Ramchapp window, ARW=Arun River valley, TRW=Tamor River Window, LW=Lumpla window, STDS, South Tibetan detachment system, KT=Kakhtang thrust, MCT=Main Central thrust, RT=Ramgarh trust, MBT=Main Boundary thrust, MFT= Main Frontal thrust. The black box is the location of the current study area. (Modified after McQuarrie et al., 2008).

margin sequences, an early Paleozoic to Carboniferous sedimentary suite and a Permian to Cretaceous sequence (McQuarrie et al., 2008).

When the Tethyan sequence was incorporated into the Himalayan orogenic wedge, the protoliths of Greater Himalayan rocks were buried at mid-crustal depths resulting in Barrovian metamorphism (Carrapa et al., 2016). The Greater Himalayan rocks were subsequently exhumed, as the hanging wall of the Main Central thrust during the early Miocene (e.g., Grujic et al., 1996; Hodges, 2000) that carried it southward juxtaposing Greater Himalaya rocks over the Lesser Himalayan sequence (Fig. 3). Concurrent to movement along the Main Central thrust, the Tethyan Himlayan sequence was detached from the Greater Himalayan rocks along the north-dipping low angle faults and zones of the South Tibetan detachment system, which marks the boundary between the two sequences (Grujic et al., 1996; Godin et al., 2006). These two opposing sense crustal-scale shear/fault systems bounding the Greater Himalayan sequence and having a coeval movement has led to several geodynamic and kinematic models such as channel flow (Grujic et al., 1996; Beaumont et al., 2001, 2004; Hollister and Grujic, 2006; Godin et al., 2006) in which, the Greater Himalayan rocks are shown as the southward extruding slab of partially molten lower to middle crust materials during the Eocene-Oligocene (Fig. 4). The Greater Himalayan rocks consist of highly metamorphosed Proterozoic to early Paleozoic metasedimentary and meta-igneous rocks (DeCelles et al., 2000; Yin, 2006; Martin et al., 2005; Parrish and Hodges, 1996; Gehrels et al., 2003, McQuarrie et al., 2008) that are intruded by both Miocene leucogranites (Fig. 5) related to the Himalayan orogenic event and Cambrian-Ordovician granites related to an older magmatic event (Tobgay et al., 2010).

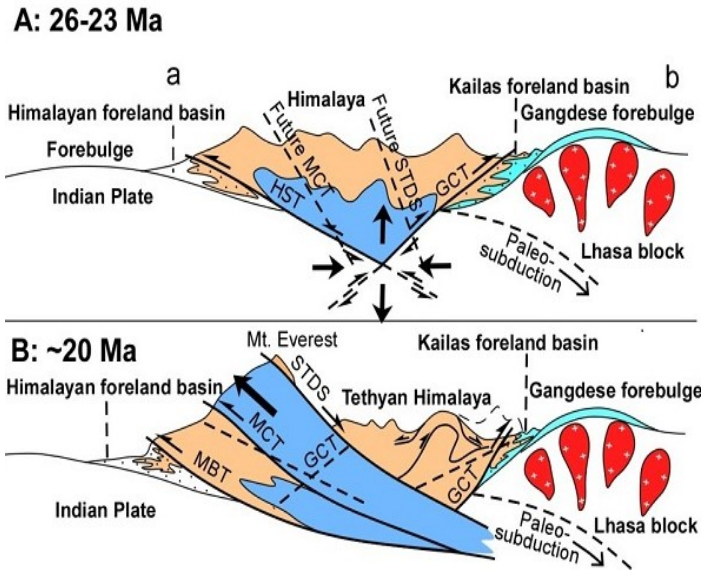

Figure 3. Schematic diagram of a proposed two-stage tectonic evolution of the Himalaya. STDS- South Tibetan Detachment system, MCT- Main Himalayan Thrust, MBT- Main Boundary thrust, GCT-Great Counter thrust. The red structure represents the granite pluton. Modified after (Wang et al., 2015).

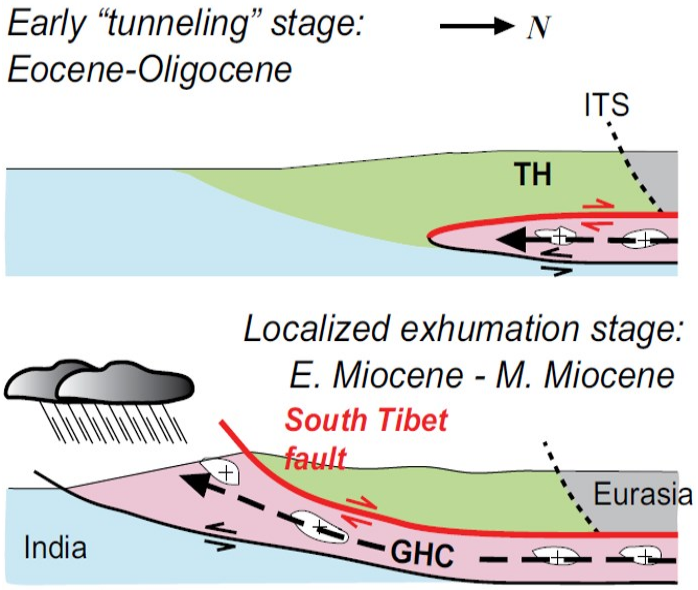

Figure 4. Schematic diagram showing Channel flow–focused denudation model. It involves two main stages; first, southward tunneling of a channel of partially molten lower and/or middle crustal rocks, and second, intensified monsoonal rains and resultant erosion forcing extrusion of these deep rocks and continued rock supply via the channel to the extruding system (Nelson et al., 1996; Beaumont et al., 2001). Modified after (Webb et al., 2017).

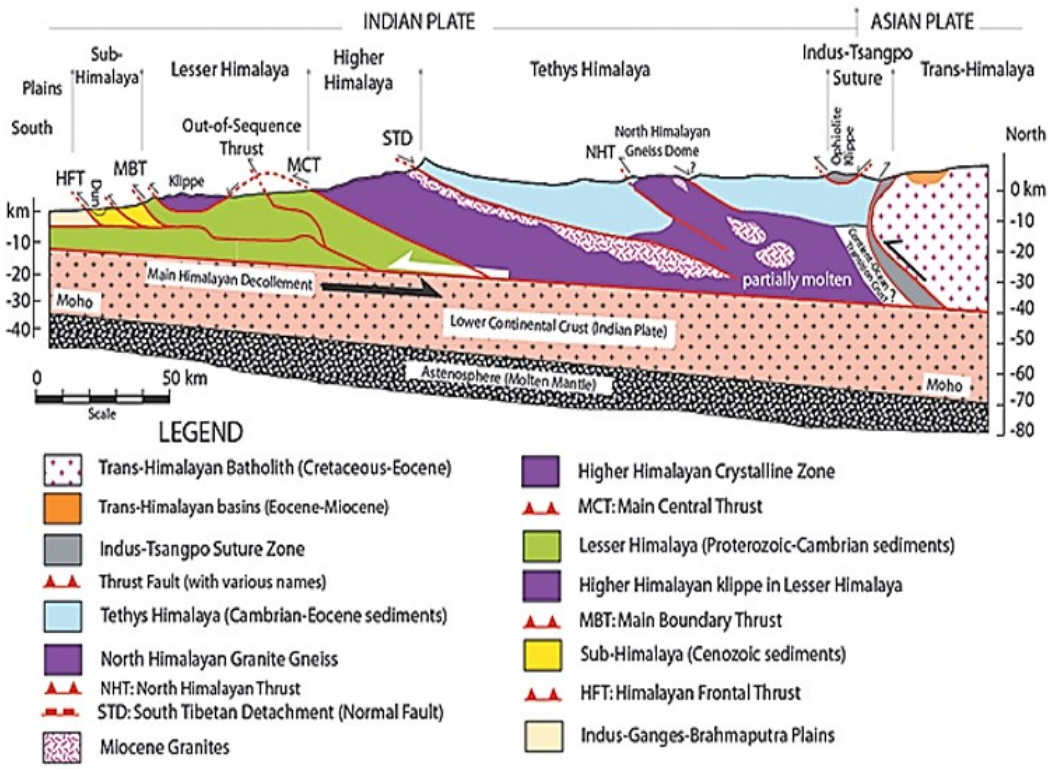

Figure 5. Structural cross-section of the Himalaya after Sorkhabi (2010). It shows the intrusion of Miocene leucogranite within the Greater Himalaya as a result of slip of the South Tibetan Detachment system. Main Frontal Thrust is denoted as HFT- Himalayan Frontal Thrust, MBT- Main Boundary Thrust, MCT-Main Central Thrust, and STD-South Tibetan Detachment.

The Lesser Himalayan sequence were uplifted and thrusted over the Sub Himalayan sequence by the Main Boundary thrust, which was thought to have been active, probably after the cessation of activity along the Main Central thrust, during the late Miocene time (Decelles et al., 2000). The Lesser Himalayan rocks represent a thick succession of clastic and carbonate rocks that covered the northern portion of the Indian craton during Proterozoic and Paleozoic time (Upreti, 1999; Myrow et al., 2003; Yin, 2006; McQuarrie et al., 2008), which were variably metamorphosed up to greenschist facies during the orogenesis (Long et al., 2011a).

The Sub Himalayan sequence contains synorogenic sedimentary rocks, formed from the shed of the growing Himalayan Mountains that were deposited during Mid-Miocene to Mid-Pliocene time (Quade et al., 1995; DeCelles et al., 1998; McQuarrie et al., 2008). This sequence, also known as the Siwalik Group, were produced by the active tectonics along the Main Frontal Thrust and marks the deformational front of Himalaya orogenic belt. The slip along the Main Frontal thrust plausibly younger than 5 Ma (Adam et al., 2016), thrusted the Siwalik Group over the modern day foreland basin sediments and have been subsequently deformed by the compressional stresses in the style of fold-and-thrust belts.

The Main Central Thrust, the Main Boundary Thrust and the Main Frontal Thrust all originate from the basal decollement known as Main Himalayan Thrust (Zhao et al., 1993; Hauck et al., 1998), which is the detachment zone that separates Himalayan orogenic wedge from the underlying Indian plate (Fig. 6).

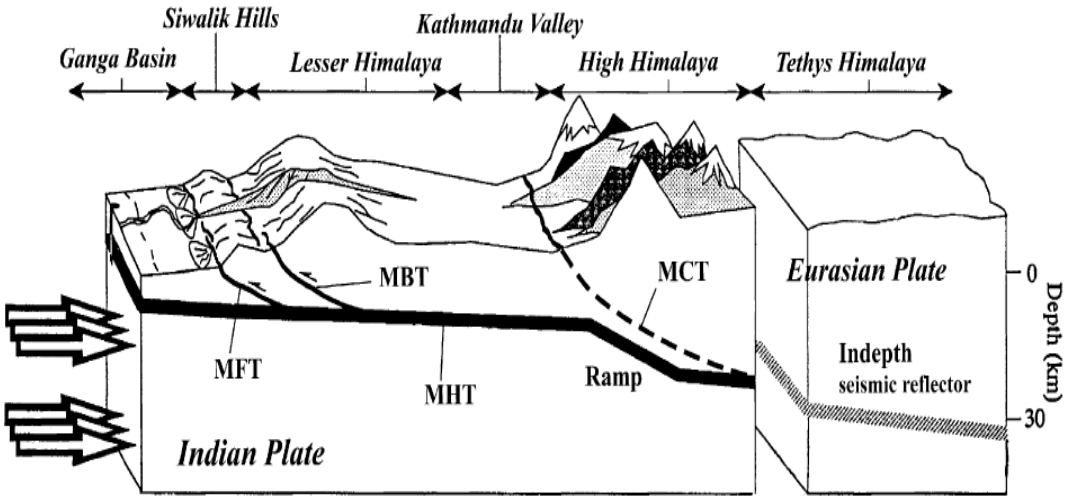

Figure 6. Schematic diagram of tectonic structures of the Himalayan orogenic belt. MFT-Main Frontal Thrust, MBT-Main Boundary thrust, MCT-Main Central Thrust, MHT-Main Himalayan Thrust (modified after Takada and Matsu'ura, 2007).

Table 1. Summary for major high strain shear zones of the Himalaya (Martin, 2017).

Name	Classification Type	Definition
Main Himalayan Thrust	Structural	Structurally lowest going through thrust along which Indian plate is underthrusting the Eurasian plate.
Main Frontal Thrust	Structural	Most frontal-vergent thrust that separates synorgonic sediments from the modern day foreland basin sediments.
Main Boundary Thrust	Structural + Stratigraphic	Most frontal foreland-vergent thrust that carried pre-Cenozoic rocks in its hanging wall.
Main Central Thrust	Structural + Stratigraphic	Foreland-vergent thrust that juxtaposed Lesser and Greater Himalayan rocks.
South Tibetan Detachment	Structural plus metamorphic	Normal dipping low-angle faults and shear zones that juxtaposed high and low grade Greater and Tethyan Himalayan rocks.

Table 2. Summary for tectonostratigraphic zones of the Himalaya (Martin, 2017).

Name	Classification Type	Definition
Sub Himalaya (Siwalik group)	Structural position	Sedimentary rocks between Main Frontal Thrust and Main Boundary Thrust.
Lesser Himalaya	Structural position	Rocks located between Main Boundary Thrust and Main Central Thrust.
Greater Himalaya	Structural and metamorphic	Rocks located in the hanging wall of the MCT and high-grade (Cenozoic peak N 600 °C).
Tethyan Himalaya	Structural and Metamorphic	Rocks located in the hanging wall of the MCT and low-grade (Cenozoic peak ≤ 600 °C).

2.2 Geology of Western and Central Bhutan.

All the major tectonostratigraphic units and the tectonic structures within the Himalayan orogenic belt are exposed in the Bhutan Himalaya (Gansser, 1983; McQuarrie et al., 2008). In addition to the antiformal tectonic window of Lesser Himalayan units exposed with the Greater Himalaya and synformal klippe of Tethyan Himalayan units, which is considered as characteristic Himalayan structures, first order local structures like Khaktang Thrust and Shumar Thrust are also mapped within Bhutan (Fig. 7).

2.2.1 Sub Himalaya (Siwalik Group). The synorogenic Neogene-Quaternary Siwalik group represent the modern Himalayan foreland fold-and-thrust belt (Coutand et al., 2016). The Siwalik in Bhutan is preserved rather intermittently, in contrast to the adjacent region, with 20-40 km portions of the belt either covered by the Quaternary Sediments, overridden by the Main Boundary Thrust, or was never been deposited (Gansser, 1983; McQuarrie et al., 2008). The Siwalik Group is litho-stratigraphically split into three members, Lower, Middle, and Upper, and in general coarsens up the section from siltstone and claystone to sandstone and conglomerates (Long et al., 2011a) (Fig. 8). The most complete Siwalik sections, up to 5 km thick, have been mapped in eastern Bhutan, where the oldest outcrops occur along the southern margin, and the youngest units near the Main Boundary Thrust (Gansser, 1983).

In central Bhutan, the Lower and Middle members of Siwalik group have been mapped within the Manas Chuu region, and the Middle member being found west of this region. In western Bhutan, only Middle member are mapped within the region of Wangchu till few kilometers east of Phuentsholing. There Siwalik Group is not exposed toward the west of Phuentsholing, and is covered by the Quaternary sediments.

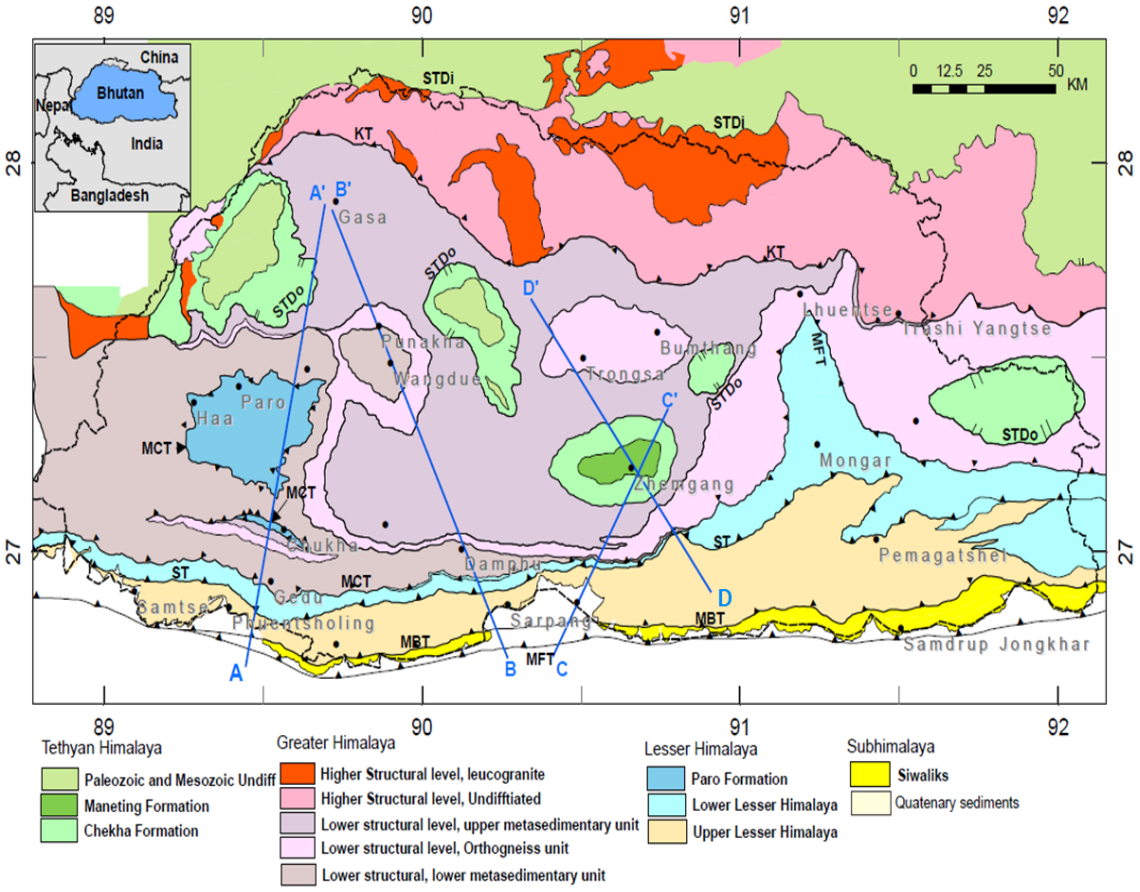

Figure 7. Simplified geologic map of the Bhutan Himalaya (modified from Long et al., 2011c). MFT-Main Frontal thrust, MBT-Main Boundary thrust, ST-Shumar Thrust, MCT- Main Central thrust, STD-South Tibetan Detachment, KT- Kakhtang thrust. The Blue lines with numbers are the profiles along in which the gravity modelling were done.

2.2.2 Lesser Himalaya. The Lesser Himalayan sequence in Bhutan, as in other part of Himalayas, is made up of a stack of thin thrust sheets Precambrian-Paleozoic rocks (Grujic et al., 1996). In the Bhutan Lesser Himalaya, another first order structure that formed approximately between 15 and 9 Ma (Long et al., 2011a) is mapped as the Shumar Thrust along which divides the Lesser Himalaya into two stratigraphic succession; the Paleoproterozoic lower Lesser Himalayan section (Shumar group), and the Neoproterozoic–Paleozoic upper Lesser Himalayan section (Baxa group) (Tobgay et

al., 2010), which are collectively 9-19 km thick (Fig. 8). The Shumar Group lies on top of this pile of allochthonous rocks and it comprises of quartzite bearing Shumar Formation, and the Daling Formation which consists of schist and green phyllite interbedded with quartzite.

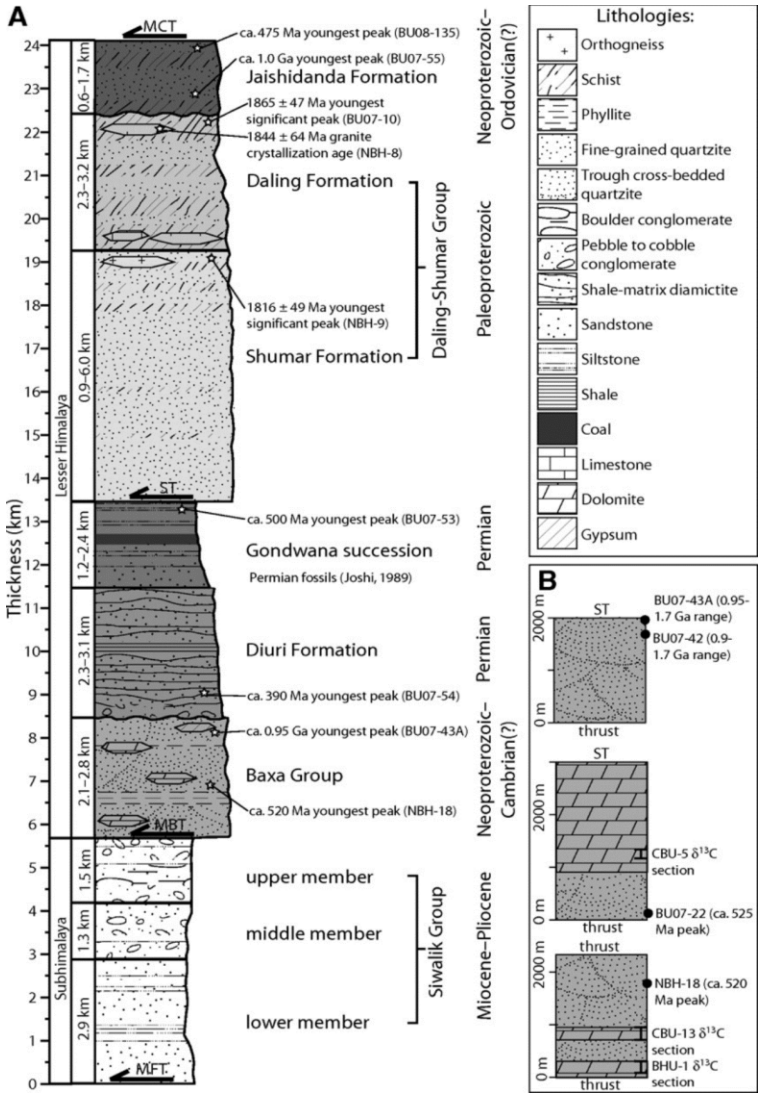

Figure 8. Stratigraphic column of Sub and Lesser Himalaya in eastern Bhutan (Long et al., 2011a). A) Column showing the tectonostratigraphy of Sub Himalayan and Lesser Himalayan units in Eastern Bhutan. B) Simplified stratigraphic column of Baxa Group Section. In western and Central Bhutan, the Diuri Formation and Gondwana Succession are not seen as it pinches out in the Eastern Bhutan (Long et al., 2011a).

The Neoproterozoic–Cambrian Baxa Group in western Bhutan is divided into the lower (Phuentsholing), and upper (Pangsari) Formations. The Phuentsholing Formation consists of slate and phyllite with interbedded limestone, dolomite, and quartzite, while the Pangsari Formation consists of talc-rich phyllite interbedded with marble and quartzite. In central Bhutan, the Manas Formation, which is composed of a medium gray, thick-bedded, coarse-grained quartzite interlayered with dark gray phyllite, marks the lower contact of the Lesser Himalayan sequence from the Siwalik Group along Main Boundary Thrust, and represents the Baxa Group. A continued occurrence of Lesser Himalayan duplex with Main Central Thrust as the thrust roof, from western to eastern Bhutan, are extensively studied are presented in the balanced geological cross-sections (McQuarrie et al., 2008; Long et al, 2011b; Tobgay et al., 2012).

The characteristic Himalayan antiformal tectonic windows exposing the younger accreted Lesser Himalayan Sequence beneath the high-grade metamorphic Greater Himalayan Sequence is expressed in general as the Paro Formation (Fig. 9). However, Tobgay et al. (2010) interpreted Paro Formation as either a single sedimentary succession of both Lesser and Greater Himalaya detritus in western Bhutan Himalaya or a complex package of isoclinally folded or thrusted strata with a unique Lesser, Greater and Tethyan Himalayan fingerprints that have been tectonically interleaved. In the absence of obvious shear zone, the boundary between the Paro Formation and Greater Himalaya zone are mapped based on the metamorphic grade and lithological contrast (Greenwood et al., 2015).

The Paro Formation (Fig. 9) consists of quartzite, quartzite–garnet–schist, marble, and minor calc-silicate rocks, which is intruded by a two mica–garnet orthogneiss

and is interpreted as the northern (distal) equivalent of the Jaishidanda Formation. This greenschist to amphibolite facies metasedimentary unit was mapped based on the presence of garnet- and staurolite-bearing muscovite-biotite schist, calc-silicate bands, and actinolite amphibolite lenses (Gansser, 1983; Tobgay et al., 2010).

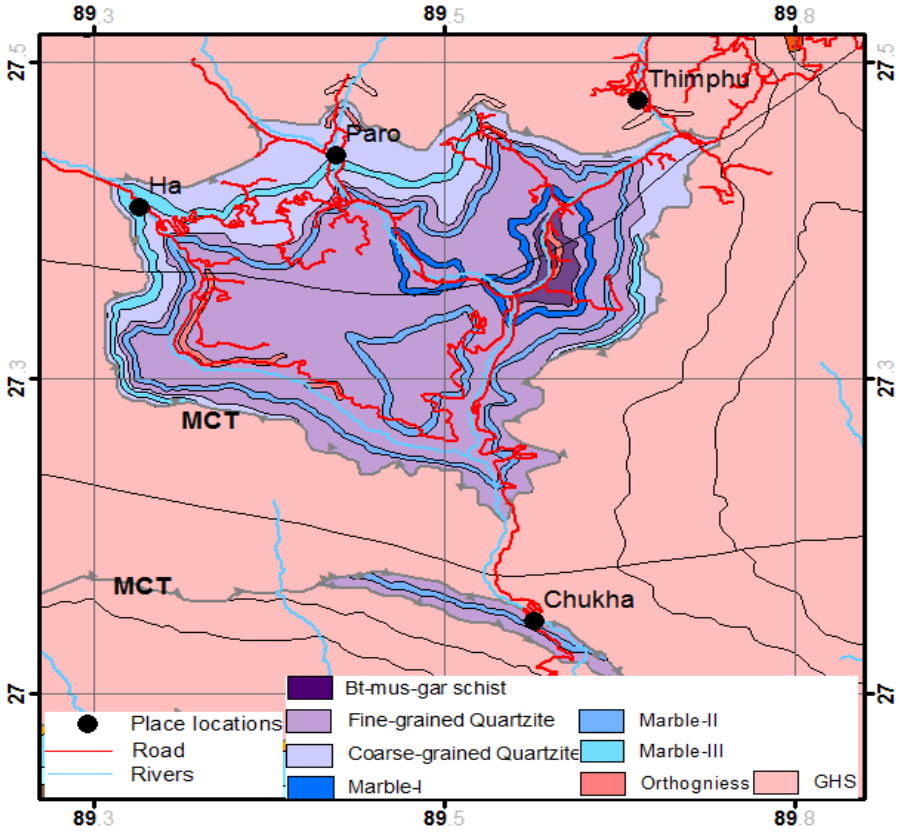

Figure 9. Detailed geologic map of Paro Formation (modified from Long et al., 2011c).

2.2.3 Greater Himalaya. Greater Himalayan rocks, which are composed of amphibolite- to granulate-facies metasedimentary, metaigneous, and igneous rocks (also known as crystalline rocks) covers much of Bhutan, an east-west trending outcrop belt that is 60-100 km wide from north to south (Gansser, 1983; McQuarrie et al., 2008, Long et al., 2011b). It is divided into lower and higher structural levels, which lay at the

footwall and the hanging wall of Kathtang Thrust respectively (Grujic et al., 2002; Tobgay et al., 2010) (Fig. 10). The higher structural level is dominated by metasedimentary rocks and magmatitic orthogenesis, and are intruded by Miocene leucogranites (Dietrich and Gansser, 1981; Gansser, 1983; Swapp and Hollister, 1991; Davidson et al., 1997, Long et al., 2011a).

The lower structural level consists of a lower Cambro-Ordovician intrusion with a granite-composition orthogneiss with metasedimentary intervals, and an upper metasedimentary unit consisting of quartzite, schist, and paragneiss (Long et al., 2011a).

The main foliation within the Greater Himalaya is affected by long-wavelength, low amplitude upright, E-W trending folds (Grujic et al., 1996) resulted from the thrust repetition of lower Lesser Himalayan strata (Long et al., 2012), two of which are in continuous with antiformal tectonic windows of the Paro Formation and the synformal klippe of the Tethayan Himalayan sequence.

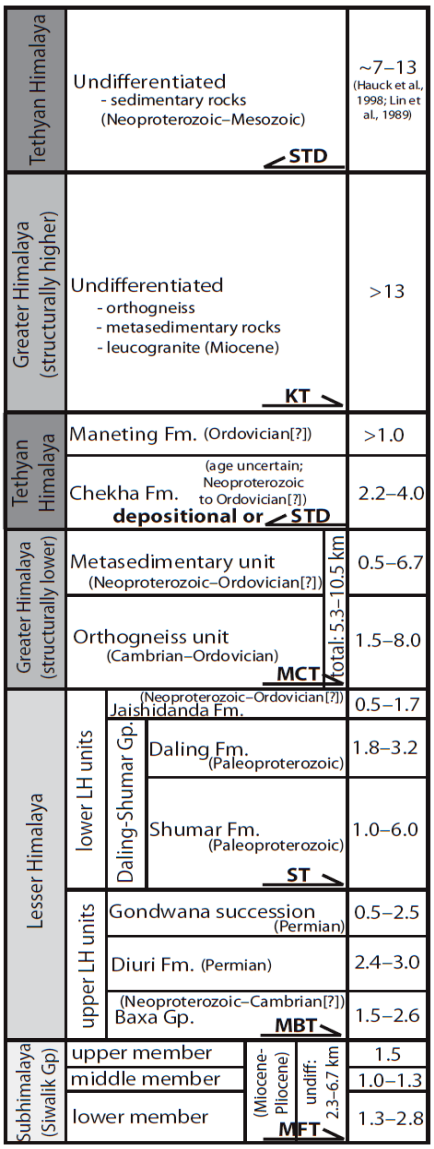

Figure 10. Geological column showing tectonostratigraphy of central and eastern Bhutan (Long et al., 2011b).

2.2.4 Tethyan Himalaya. Exposed Precambrian through Mesozoic rocks of Tethyan Himalayan sequence, is well

preserved in Bhutan above the Greater Himalayan sequence as synformal klippe (Gansser, 1983; Tobgay et al., 2010; Long at el, 2011b) (Fig. 10). The Chekha Formation that forms the base of TH rocks, consists of quartzite interbedded with biotite-muscovite-garnet schist (Long et al., 2011b). These rocks are overlain by the Maneting Formation, which is composed of phyllite and fossiliferous limestone of Late Cambrian age and locally known as the Wachi La Formation (Tangri and Pande, 1995; Hughes et al., 2010; Tobgay et al., 2010). There are two segments of South-Tibetan Detachment system in Bhutan, internal north segment referred to as inner South Tibetan Detachment system and more external south segment known as outer South Tibetan Detachment system. Although, defining the South Tibetan Detachment system in Bhutan has been considered debatable (Long et al, 2017), the Chekha Formation is preserved within the outer-South Tibetan Detachment system (Kellett et al., 2009). However, Long and McQuarrie (2010) have argued that the South Tibetan Detachment system is absent in the Tethyan sequence in Central Bhutan (Zhemgang region).

3. PREVIOUS GEOPHYSICAL STUDIES

3.1 Seismic Studies in Eastern Himalayan Orogeny

One of the earliest seismic explorations have been the deep seismic reflection data acquired by project INDEPTH (International Deep Profiling of Tibet and the Himalaya), where the seismic data were acquired within the southern part of the Yadong-Gulu rift in the southern Tibet (Fig. 11). The deep seismic reflection data from the project INDEPTH have been interpreted by various authors (Zhao et al., 1993; Hauck et al., 1998) to unravel the structure of the crust and upper mantle beneath southern Tibet and in the northern region of Sikkim-Bhutan Himalaya.

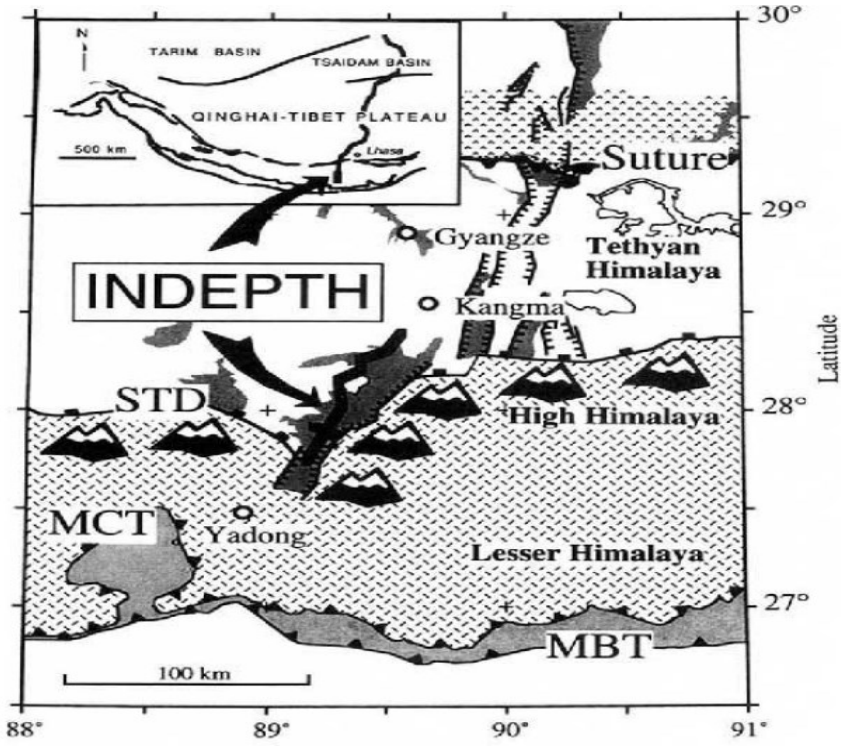

Figure 11. Simplified geologic map showing the location of INDEPTH Pilot deep seismic profile modified after (Zhao et al., 1993). MBT-Main Boundary thrust, MCT- Main Central thrust, STD-South Tibetan Detachment.

Zhao et al. (1993) first interpreted the results from these data by constructing an image of the active mid-crustal thrust fault along which Indian plate is being underthrust beneath southern Tibet, geometries indicating large scale structural imbrication of the upper crust, and the configuration of Moho boundary (Fig. 12). These results supported the concept of crustal thickening beneath southern Tibet was caused by the underthrusting of Indian continental crust.

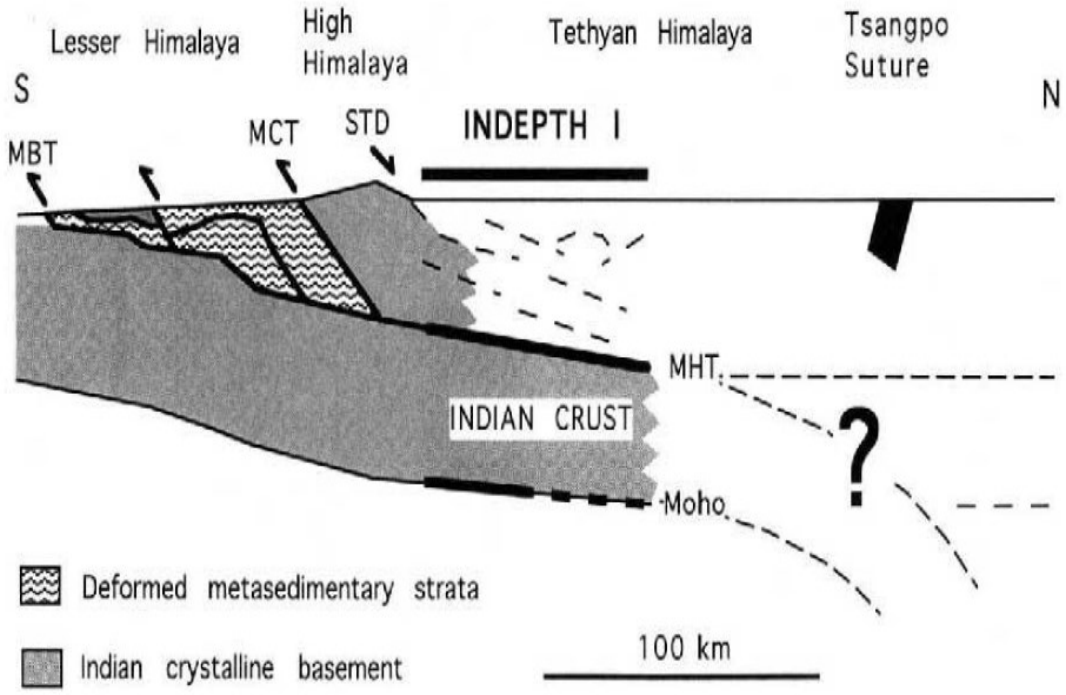

Figure 12. Schematic crustal cross-section of the Himalayan and the southern Tibetan Plateau showing the location of the location of INDEPTH seismic profile with large-scale crustal structures derived from it. The Upper crustal crustal-structure towards the south of the crest of Himalaya was generalized from Schelling (1992). MBT, MCT, MHT, STD, are defined in Fig. 11. Modified after Zhao et al. (1993).

Hauck et al. (1998) also interpreted the data from the INDEPTH project and emphasized that at ~90^{o} E longitude, the decollement, an active mid-crustal thrust fault,

marking on top of underthrusting Indian crust was dipping north to ~28.6º N and to the depth of ~45 km, which were interpreted as the large north dipping ramp in the decollement (Fig. 13). The study also showed the contact between the Tethyan and the Greater Himalayan sequence in between Bhutan Himalaya and Kangmar dome are represented by the South Tibetan Detachment, which was found continuous in the subsurface. Furthermore, the study suggested that the Indian mantle lid underthrusts Tibet to approximately the middle of the plateau.

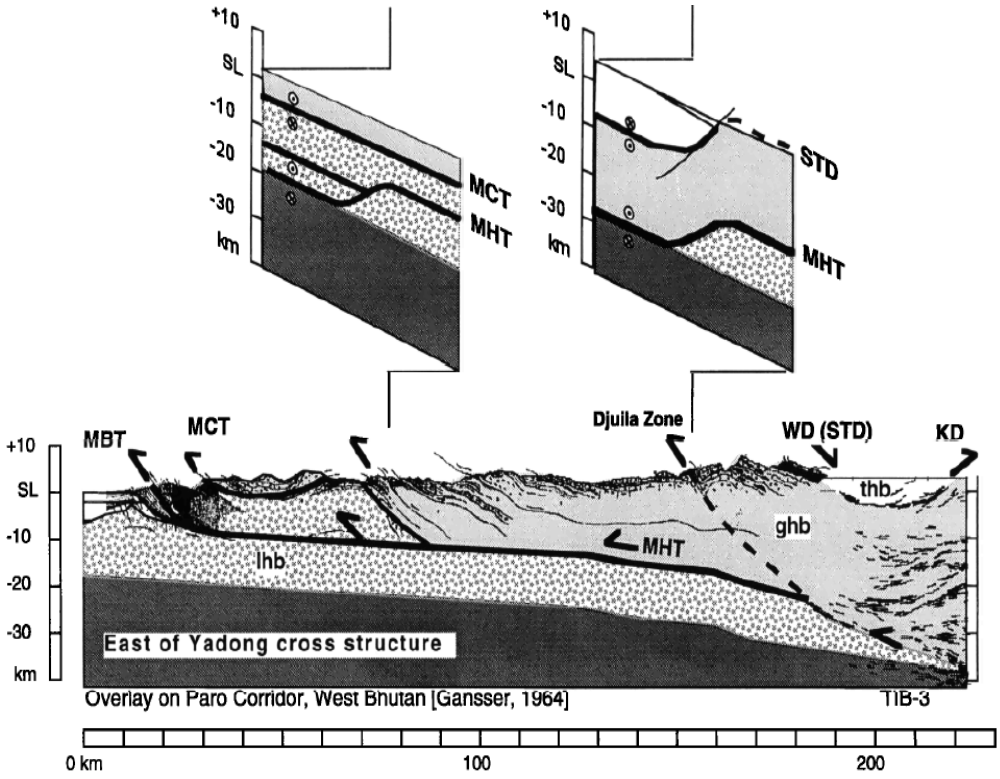

Figure 13. Interpretive geologic cross-section across the western Bhutan Himalayan. This is constructed in combination of a geologic cross section (Gansser, 1964) and the results from INDEPTH seismic reflection profile. MBT-Main Boundary thrust, MCT-Main Central Thrust, MHT-Main Himalayan Thrust, STD-South Tibetan Detachment, and KD-Khangmar Detachment. Modified from Hauck et al. (1998).

However, as the deep seismic reflection data from the project INDEPTH were mainly focused in the southern Tibetan and the northern part of the Himalayan orogeny, all the above interpretation are mostly limited to those regions and have very low resolution about the subsurface structures beneath the southern (Lesser Himalaya and Subhimlaya) part of the orogeny.

3.2. Seismic Studies in Central Himalayan Orogeny

Lithospheric deformation beneath the Himalayan orogeny were also investigated using broadband seismic data from the Himalayan Tibetan Continental Lithosphere during Mountain Building (Hi-CLIMB) project conducted along Nepal and Tibet (Fig. 14) (Nábělek et al., 2009).

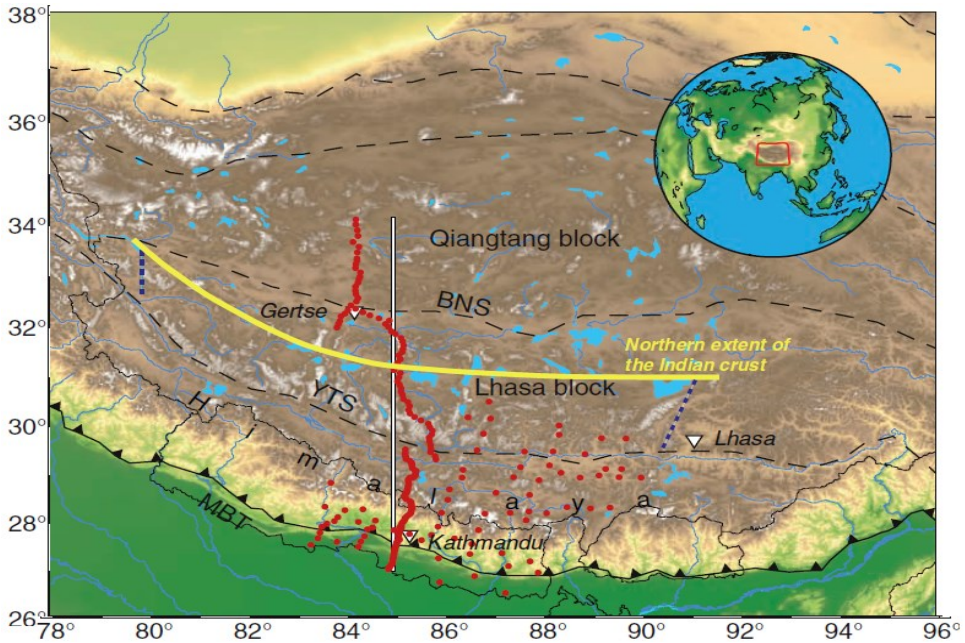

Figure 14. Location map of Hi_CLIMB experiment in Nepal and on the Tibetan Plateau, where red circles indicate the positions of broadband seismological stations. The cross section along the profile (White line) is shown in Fig. 15. Modified after Nábělek et al. (2009).

Using receiver function methods, (Nábělek et al., 2009) have constructed an image of the crust and upper mantle beneath the Himalayas and the southern Tibetan Plateau, where Moho geometry is imaged at 40km beneath Ganga basin, 50 km beneath southern Himalaya and reaching upto 70 km beneath Greater Himalaya. The study revealed a continous geometry of Main Himalayan Thrust which has a shallow depth under Nepal to the midcrust under southern Tibet (Fig. 15). It also shows 15 km thick of underplated lower crust and an anisotropic crust/mantle interface beneath the Tibet indicating shearing during the deformation.

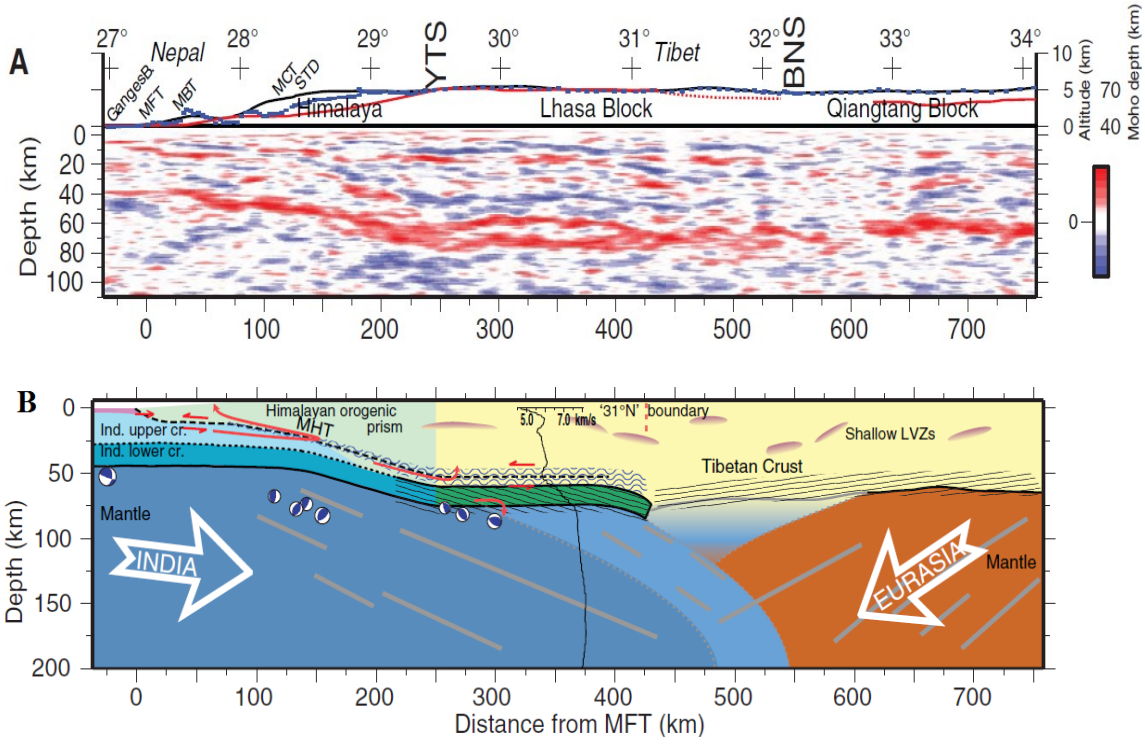

Figure 15. Receiver function image and interpretive geologic cross-section of central Himalaya at longitude ~85^{0}E (modified after Nábělek et al. (2009). A) Receiver function image showing the principle boundaries within the lithosphere (red and blue colors represent interfaces with increasing and decreasing impedance with depth, respectively), where red lines indicates Moho depth. B) Interpretive cross section of India-Eurasia collision zone. Eclogitized lower crust is shown in green, the crust-mantle boundary is the thick black line when strong and gray when weak. MHT-Main Himalayan Thrust.

3.3 Seismic Studies in Bhutan Himalaya.

To decipher the lithospheric structures beneath the Bhutan Himalaya, the Geodynamics And Seismic Structure of the Eastern Himalaya Region (GANSSER) experiment was conducted between January of 2013 and November of 2014 by deploying a temporary broadband seismic network. The network consisted of 38 broadband seismometers that were arranged in two densely spaced south-north arrays in western and eastern Bhutan (Fig. 16), with a station interval of 7-8 km. Data from this experiment were analyzed for receiver functions (RFs) to map deep structure and ambient noise tomography (ANT) to map upper crustal structures.

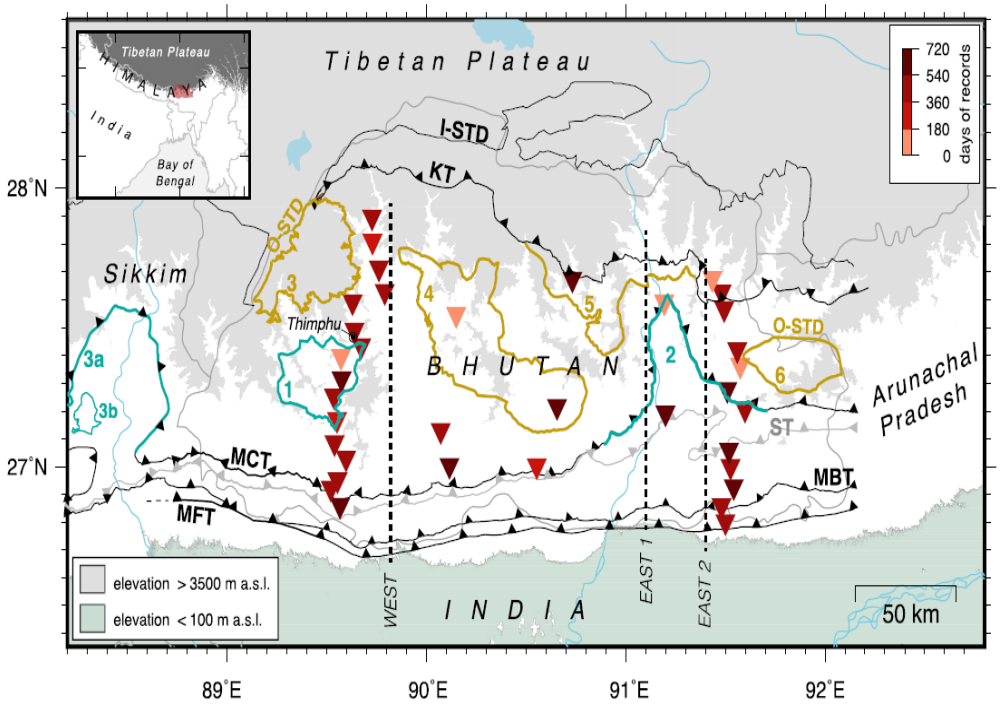

Figure 16. Map of the Bhutan Himalaya with location of the broadband seismic stations of GANSSER network (red triangles) (Singer et al., 2017b). Main tectonic structures including MFT- Main Frontal thrust, MBT- Main Boundary thrust, MCT- Main Central thrust, KT- Kakhtang thrust, I-SDT-Inner South Tibetan Detachment, O-STD- outer South Tibetan Detachment are shown.

The broadband seismic data from the GANSSER temporary network were used to create Receiver Functions using a 3D migration algorithm to image lithospheric structures (Singer et al., 2017a). Receiver Functions from the individual stations were first converted to time-depth function using minimum 1D P- and -S wave velocity model to approximate the Moho depth. This model also provided information about possible intra crustal discontinuities. Then, to accurately image the crustal structures and intra crustal features, an iterative 3D migration algorithm to create Receiver Functions was applied to the velocity model, which estimated that the Moho to be present at a depth ranging between 50 and 75 km with abrupt steeping from shallow angle of $\leq 3^{o}$ from south still 27.3^{o} N to ~18^{o} towards the north from thereafter in western Bhutan in contrary to ~50 km sub horizontal in eastern Bhutan (Figs. 17 and 18). In addition to

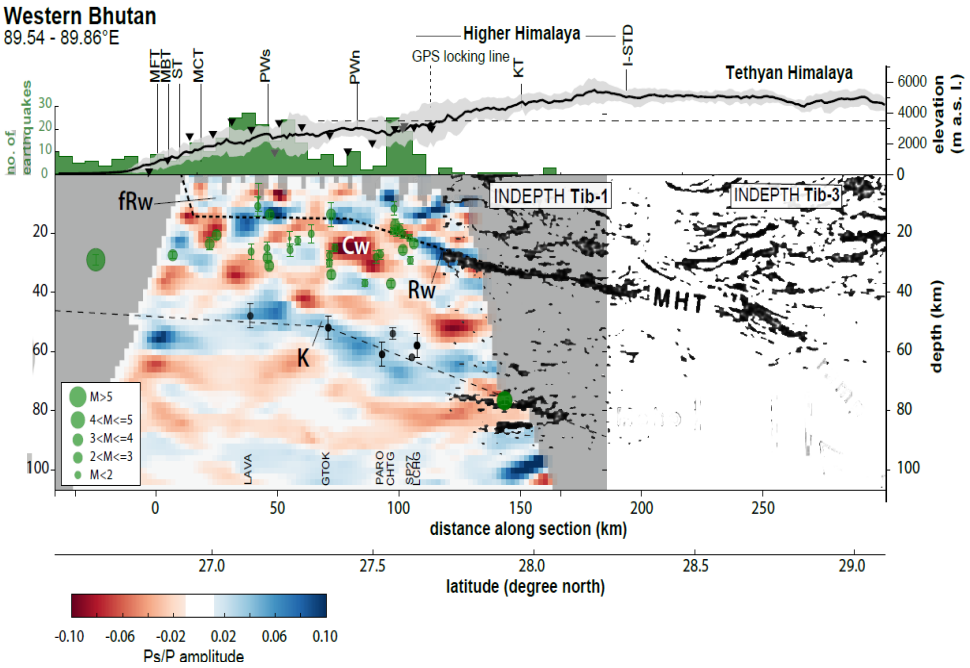

Figure 17. 2-D stack of individual cross-sections obtained from the 3D migration image of radial RF's in western Bhutan (Singer et al., 2017a). MHT-Main Himalayan Thrust, K-kink in Moho Geometry, Cw-intracrustal converter, fRw-frontal ramp of MHT and Rw-mid-crustal ramp of MHT. MFT, MBT, MCT, KT, I-STD, same as Fig. 16.

the Moho geometry, ramp-like structures of Main Himalayan Thrust dipping 18° northward at the depth of 30 km beneath Greater Himalayan sequence was also imaged, whereas, beneath the Subhimalaya and the Lesser Himalaya sequences, sub horizontal Main Himalayan thrust were mapped at around 14 km depth.

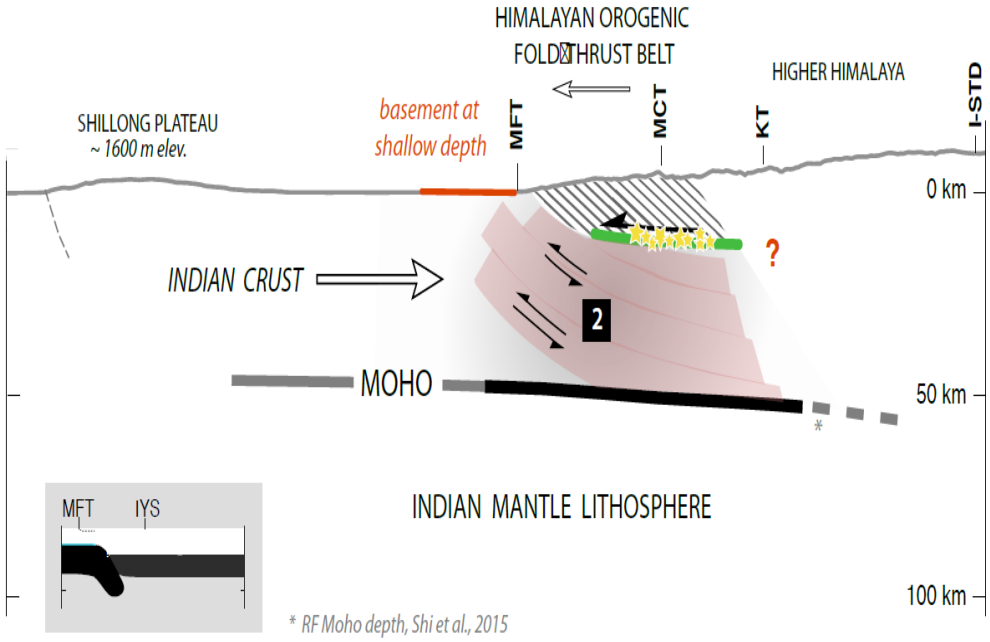

Figure 18. Tectonic model of eastern Bhutan (Singer et al., 2017a). Thick black line represents the Moho geometry determined from GANSSER broadband seismic data and thick green line represent plausible Main Himalayan Thrust. MFT, MCT, KT, as same as in Figs 16 and 17.

Ambient noise tomography seismic data was calculated to produce surface wave tomography maps (Singer et al., 2017b). Ambient noise tomography analyzes short period surface Rayleigh waves to determine the velocity variations within the crust. Data quality was evaluated by calculating Rayleigh-wave group velocities in the periods between 2-20 seconds to produce 2D group velocity maps (Fig. 19). Subsequently, these measurements were directly inverted for 3D shear wave velocity structures by using a

direct inversion scheme. With this method, upper crustal structures up to 18 km depth beneath Bhutan were mapped (Fig. 14). Singer et al. (2017b) proposed that the high shear wave velocities (>3.6 km/s) beneath the Paro window and on top of mid-crustal ramp of Main Himalayan thrust could be related to Lesser Himalayan quartzite dominated rocks or felsic migmatites with large intrusion of leucogranites.

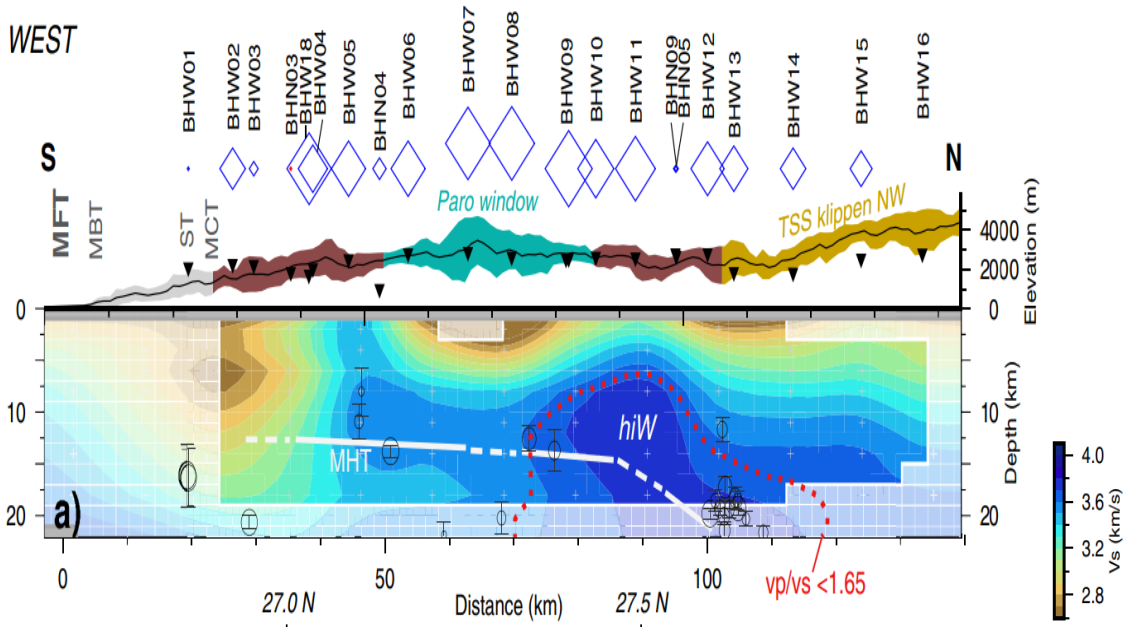

Figure 19. Shear-wave velocity variations across the orogenic wedge and in relation to the tectonic surface structure (Singer et al., 2017b). MHT-Main Himalayan thrust, hiW-the high velocity anomaly in western Bhutan. MFT, MBT, MCT, as same in Figs. 16 and 17.

3.4. Gravity Studies in Nepal and Indian Himalaya

A number of large scale gravity modelling studies have been done in the adjacent Himalayan region such as in northwest (NW) of Nepal (Chamoli et al., 2010), in Nepal and Sikkim-Darjeeling (Ansari et al., 2014) (Fig. 20), and the Himalaya and Lhasa block (Bai et al., 2013), which provide a preliminary insight on the nature of crustal structures

that could possibly be found beneath the Bhutan Himalaya.

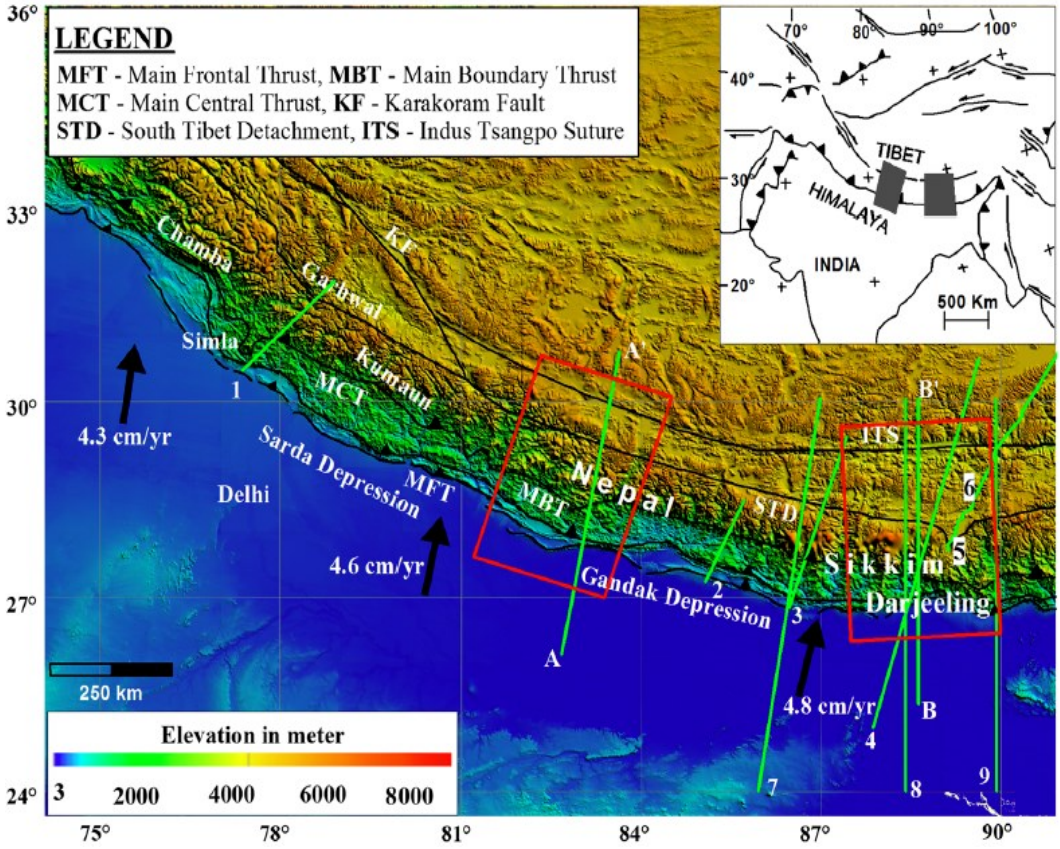

Figure 20. Simplified tectonic map with the gravity profile and the overview of topography of Nepal and Sikkim-Darjeeling Himalayas (after Ansari et al., 2014). Various profiles from the previous studies (profile 1-9) were used to constrain the initial lithosphere geometries along the profile AA' and BB' shown in the (Fig. 19).

The 2D forward modelling of the gravity anomaly data beneath Nepal and Sikkim-Darjeeling (India) by Ansari et al. (2014) shows a similar lithospheric structure to the aforementioned seismic studies, and the flexure of Indian plate beyond the Main Boundary Thrust and reaching a maximum depth between the Main Central Thrust and South Tibetan Detachment system in both the areas. However, a steeper of the Moho boundary is noted in the Sikkim-Darjeeling area then in Nepal (Fig. 21).

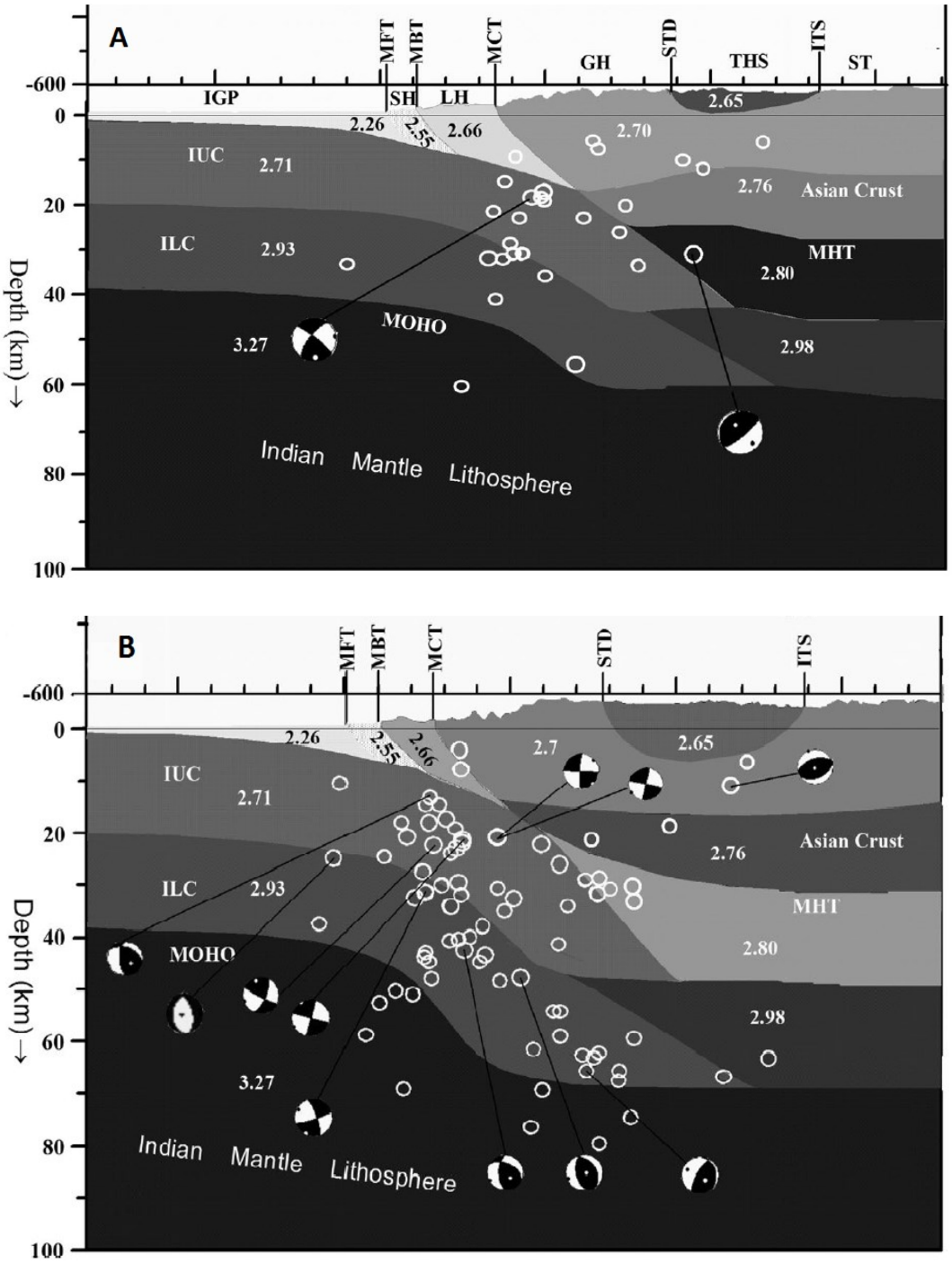

Figure 21. 2-D gravity models in Nepal and Sikkim-Darjeeling region (after Ansari et al., 2014). It shows hypocenter represented by white circle and focal mechanisms. A) Nepal and B) Sikkim-Darjeeling. SH- Subhimalaya, LH-Lesser Himalaya, GH-Greater Himalaya, TH-Tethyan Himalaya, ITS-Indus Tsangpo Suture. MHT, MFT, MBT MCT, STD, same as in Figs. 16 and 17.

In the NW Nepal, (Chamoli et al., 2010) constructed 2D gravity forward model of the a lithosphere constrained by results from a 2D spectral analysis (power spectrum of Bouguer gravity anomaly) that suggested three density layer interfaces corresponding to the Main Himalayan Thrust, the Conrad discontinuity and the Moho boundary (Fig. 22). The model indicates the Moho depth increasing from 45 to 80 km towards the north with the locus of flexure of Indian crust beneath the Greater Himalayan sequence.

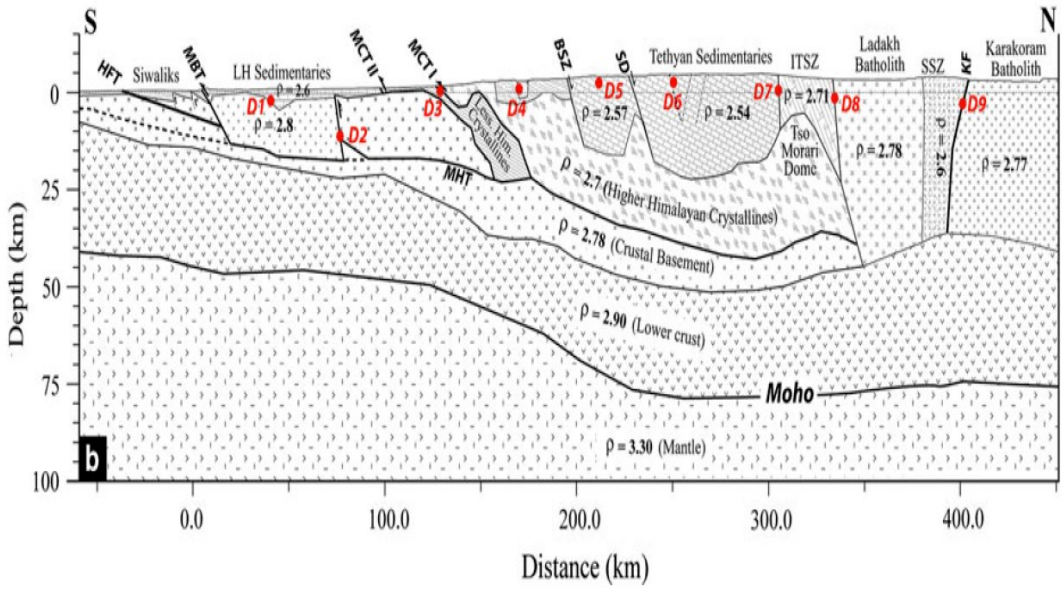

Figure 22. Gravity model across the northwest Himalayan orogeny. Constraints were derived from a gravity-based power spectrum, coherence method, and wavelet analysis and geological information. The geometry of the shallow structures were constrained by wavelet analysis and densities are in g/cc. Modified after Chamoli et al. (2010). HFT-Himalayan Frontal Thrust, and MHT, MBT, MCT are same as Fig. 21.

3.5. Gravity Studies in Bhutan Himalaya

No detailed gravity subsurface modelling has been, as of yet, conducted in Bhutan .Only a gravity analysis at a regional scale was conducted to study the flexure of Indian plate beneath Bhutan (Hammer et al., 2013) by acquiring gravity data at 214 locations

(Fig. 23). Using a 2-D thermomechanical model, the study suggested the upper mantle as the strongest continental lithosphere beneath Bhutan and observed east-west decrease in flexural wavelength associated with weakening of mantle rheology.

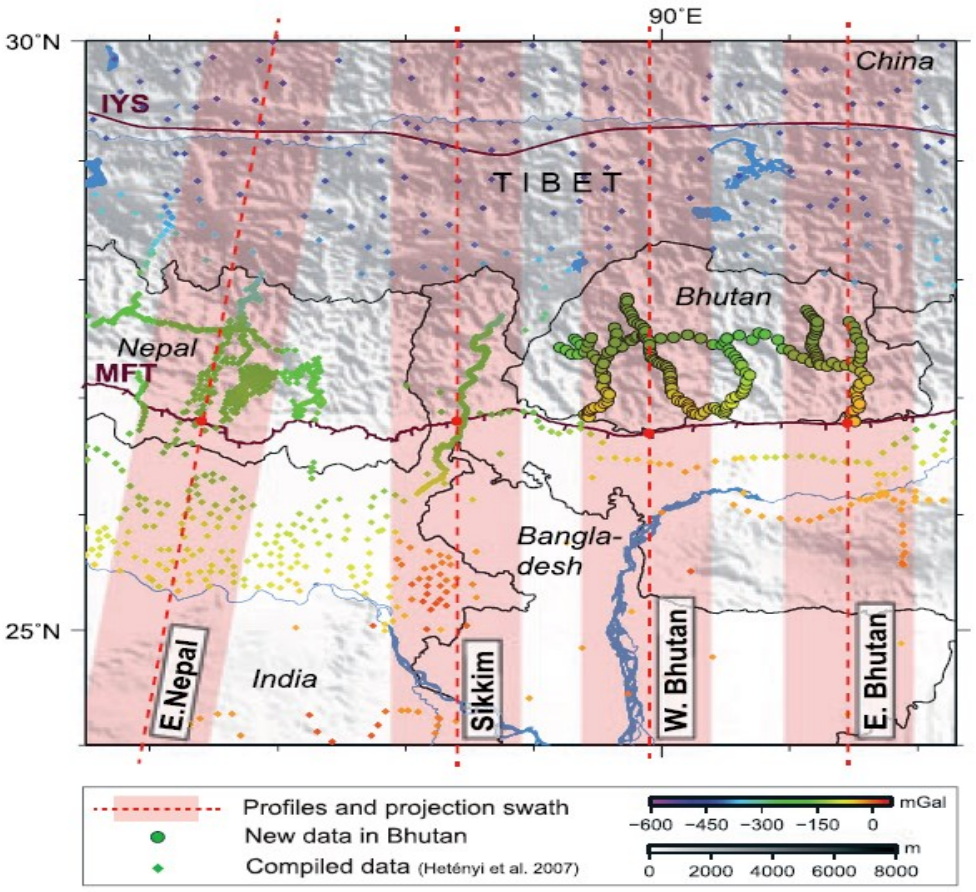

Figure 23. Map showing existing gravity data in Bhutan (Hammer et al., 2013). Gravity data (circles) in Nepal and India are also shown.

4. GRAVITY DATA COLLECTION AND PROCESSING

4.1 Gravity Data Collection

A detailed gravity survey was conducted during two field seasons; 1) November 2015 through January 2016 in western Bhutan, 2) November 2016 through January 2017 in central Bhutan. Approximately 2300 gravity stations in total were acquired using Lacoste & Romberg model G gravimeter and dual frequency differential GPS receivers. The observations were taken along all major roads with the station interval ranging from 500 m to 1000 m (Fig. 24).

At each station, at least two gravity measurements (meter readings), and 15-20 minutes of GPS observations using a dual frequency Topcon GRX-2 GNSS and Trimble 5700 series GPS receiver were collected. In order to obtain centimeter accuracy in elevations, GPS reference stations were established in order to post process the field data. At each of these reference stations, between 8 and 10 hours of GPS observations were recorded using a Trimble 5700 GPS receiver to obtain centimeter accuracy reading at the reference station. These data were processed using the single station method via proprietary algorithm provided by the National Imaging and Geospatial Agency. Not all the field gravity stations and their GPS recordings used the temporary GPS reference stations but the Permanent Reference Station (PRS) data from stations in Bhutan that were operated by the National Land Commission Secretariat, and stations in northern India and eastern Nepal that were acquired through online were also used. The spatial coordinates and ellipsoidal elevations of the all the gravity stations were obtained through differentially correcting the field GPS data by post processing in the Topcon Tool

software with the GPS reference stations. The horizontal and vertical accuracy of sub-meter level were accomplished for ~99% of the gravity stations. For few gravity stations (around 10 stations) the vertical accuracy was limited to ~ 1-2 m due to the dense vegetation blocking the satellite signals.

Fourteen gravity base stations were established at easy to locate sites which were reoccupied at least twice in a day. These repeated readings were performed in order to account for the drift of the instruments that occur with time due to elastic creep within the meter's spring and also to help remove the gravitational effects of the earth's tides. There were several of these local base stations that were occupied during the survey. All the base stations were tied to the first local base station was located outside the office of the Department of Geology and Mines. During the course of the survey, the local base stations were occupied multiple times and retied into the local base station in Thimphu. The process increased the accuracy of the local base stations. The local gravity station at the office of Department of Geology and Mines was tied to absolute gravity base station located at the office of National Land Commission Secretariat (NCLS) in Thimphu, Bhutan by taking several gravity measurements at the site. This was done in order to merge our data into the 1971 gravity standardization net (Morelli, 1976).

4.2 Gravity Data Processing

The meter reading from the gravimeter is not an absolute gravitational acceleration, but a recording expressed in meter units. The meter units were calibrated (into mGal) by multiplying it by the meter constant. After the calibrations, local gravity base stations were first adjusted to an absolute gravity value using the absolute gravity

reading that was recorded in Thimphu, and then this adjustment was applied to all the other gravity stations. In order for these observed gravity data to be interpreted in terms density variation caused by the subsurface structures, all known gravitational effects that are not related to the subsurface density changes must be removed.

The first correction is remove any instrumental drift that occurred during each day's readings. The local base station was occupied as the first and last station each day. Since the reading will change slightly during the day due to stretching of the spring. A linear drift was constructed between the two local base stations and the amount of change as a function of time was determined and either added or subtracted to each field reading.

To remove the effects of Earth's shape, mass and rotation, the 1967 International Gravity Formula (Morelli, 1976) was designed to calculate to theoretical/ normal gravity values over the surface of Earths reference ellipsoid, which is a function of the geographical latitude of the site. Normal gravity at each gravity station was determined with its corresponding latitude, and then subtracted from the observed gravity to obtain observed gravity anomaly. This process is known as latitude adjustment.

Gravity also depends on the elevation of where the gravity reading was located. The change in gravity with elevation is around 0.3086 mGal/meter, in other words, there is an inverse relationship between the elevation and the gravity. To account for gravity variations due to change in elevation, a free air anomaly was computed using mean sea level as datum. As the name suggests, in free-air correction (FAC), we postulate that only air fills the space between the station and the datum, without any mass. To compensate for the mass of rock that lies above the datum, a Bouguer gravity correction was made.

The Bouguer gravity correction assumes the land mass above the datum is an

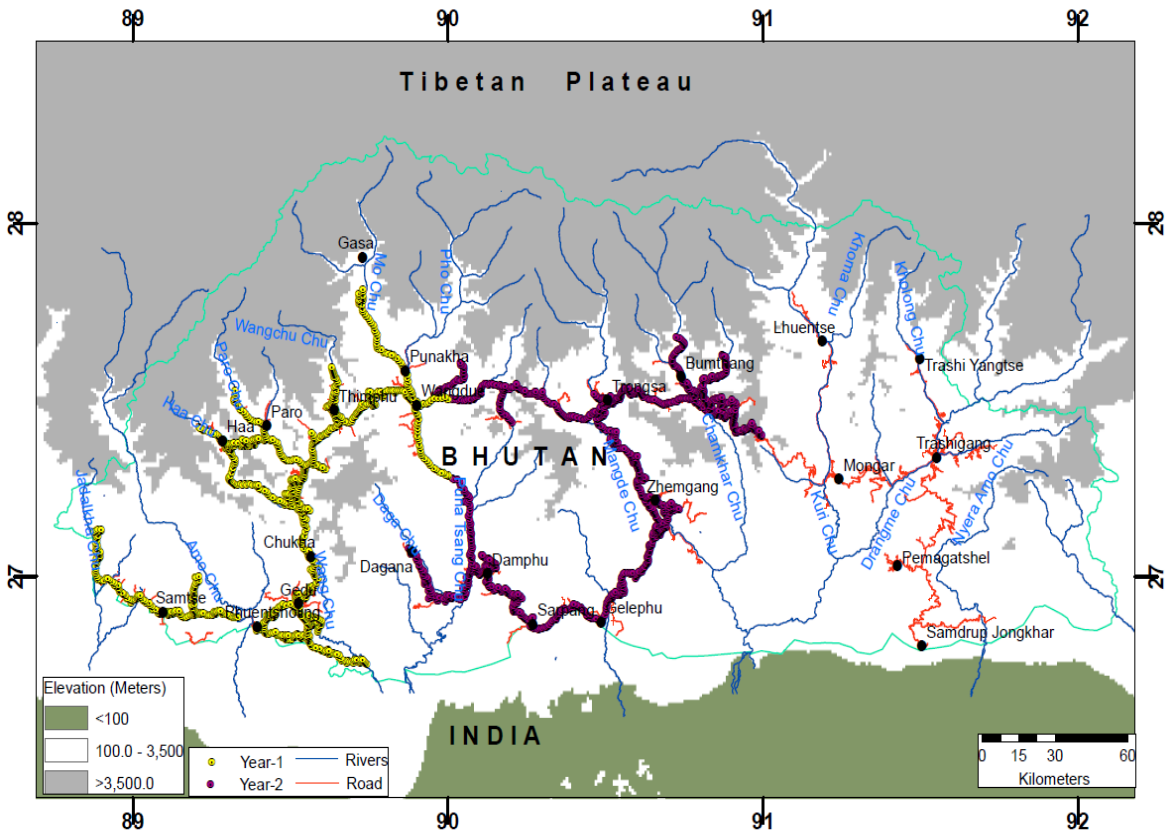

Figure 24. Elevation map of Bhutan showing the gravity stations. Gravity stations from the first year (2015-2016) in western Bhutan is shown in yellow and from the second year (2016-2017) in purple.

infinite horizontal plate of thickness *h* with the density ρ. A Bouguer gravity anomaly was computed using reference/reduction density of 2.67 g/cm^3. All the corrections and adjustments mentioned above, including instrument drift and earth tide corrections, were all performed using a computer algorithm (FORTRAN program) written by Dr. Kevin L. Mickus.

For a rugged terrain like in Bhutan, the assumption of a flat horizontal land mass between station and the datum is not sufficient. A gravimeter occupied at an observation site is not only attracted by the mass of earth beneath it, but also affected by to the

upward attraction of the nearby hills that rise above it and the lack of mass in nearby valleys. Therefore, terrain adjustment is required for each station. Terrain corrections were performed using the GeoSoft Oasis Montaj software using the 10 m Advanced Land Observing Satellite (ALOS) digital elevation model (DEM) as the local terrain grid, and the 90 m Shuttle Radar Topography Mission (SRTM) DEM as the regional terrain grid and 2.67 g/cm^3 as the density of surface rocks. Gravity variation of maximum ~69 mGal and minimum of ~5m Gal was recorded from the terrain corrections (Fig. 25), which were then added to the Bouguer gravity anomaly to finally obtain a complete Bouguer gravity anomaly.

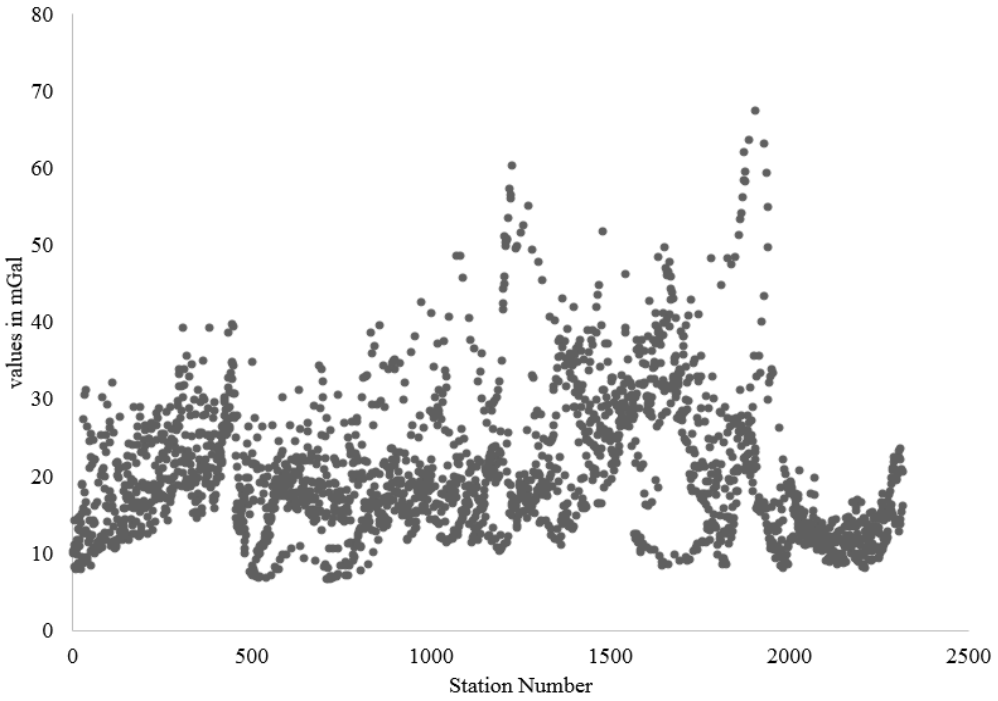

Figure 25. Graph showing the variation in gravity at each station caused by the terrain.

5. GRAVITY DATA ANALYSIS

5.1 Bouguer Gravity Anomaly Map

The complete Bouguer gravity anomaly data obtained after applying all the above corrections were gridded with 1 km interval using a minimum curvature algorithm to prepare the Complete Bouguer gravity anomaly map (Fig. 26). The Bouguer gravity anomaly observations in western and central Bhutan show prominent gravity minima, with decreasing values from the Lesser Himalaya towards the Greater Himalaya. It is observed that the northernmost and southernmost extent of the data coverage records the minimum and the maximum gravity anomaly respectively. A minimum of (-378 mGal) was recorded in the Gasa region while the maximum value of (-128 mGal) is seen to the east of Phuentsholing region. This shows an inverse correlation between the Bouguer gravity anomalies and the elevation (Fig. 27). Simpson et al. (1983, 1986) explained that this inverse correlation is primarily caused by a regional mass deficiency at deep crustal depths that supports the topography according to the theory of isostasy, and Lyon-Cyan and Molnar (1985) suggested that the Lesser and Greater Himalayas along the entire length of the Himalaya are considered undercompensated.

The observed Bouguer gravity anomalies correspond to the regional scale density variations which are not in general related to the near surface lateral density variation. Consequently, a distinct line of separation between the different tectonostratigraphic zones of the area are not revealed by the gravity anomalies. In general, the Bouguer gravity anomalies in the Lesser Himalayan zone have relatively higher values, ranging on average between -128 and -230 mGal, than the other zone, which may be related to the

densities of these lithologies. The correlation between the Bouguer gravity anomalies and the geological units is reflected in Fig. 28. The Lesser Himalayan zone, particularly in the central part of the study area, several regions of gravity maxima, (anomaly 1) (Fig. 26) are observed which could possibly be caused by high density quarzitic rocks units. Further towards the north, the Greater Himalayan regions record the lowest amplitude anomalies with values ranging between -160 and -375 mGal (Fig. 28). This decreasing values are caused due to thickening of the crust up to 70 km beneath it resulting in the abrupt increase in the topography (Lyon-Caen and Molnar, 1985; Tiwari et al, 2015). There is no definite range of gravity anomalies observed to define for the Tethyan Himalayan zone, because this geologic units occurs at different location within the Greater Himalayan zone as klippe.

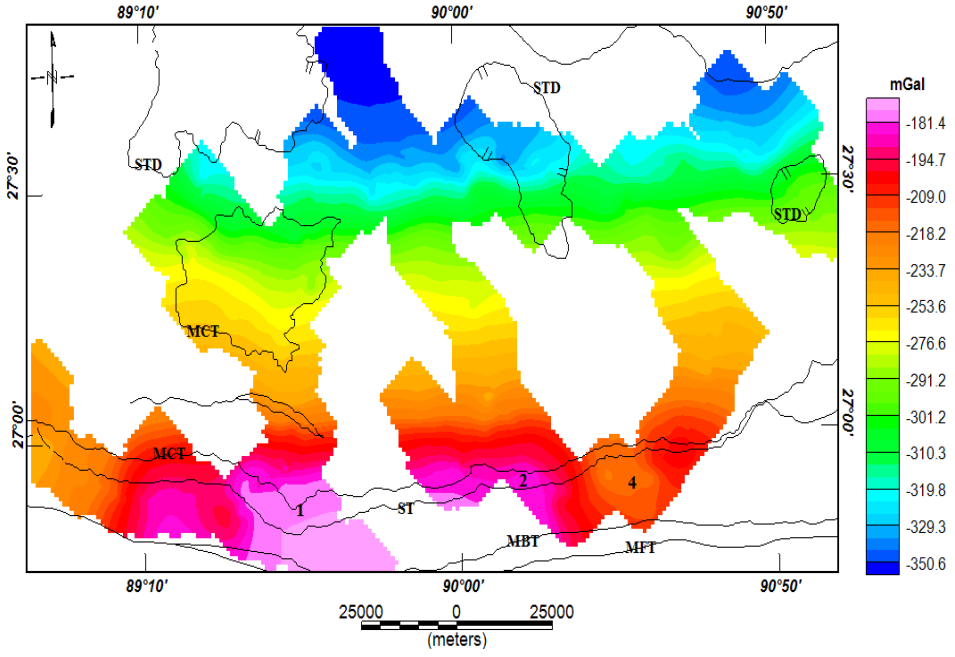

Figure 26. Complete Bouguer gravity anomaly map with large scale geologic units outlined in black. MFT- Main Frontal Thrust, MBT-Main Boundary Thrust, MCT-Main Central Thrust, STD- South Tibetan Detachment, and KT-Kaktang Thrust. Numbers represent anomalies discussed in the text.

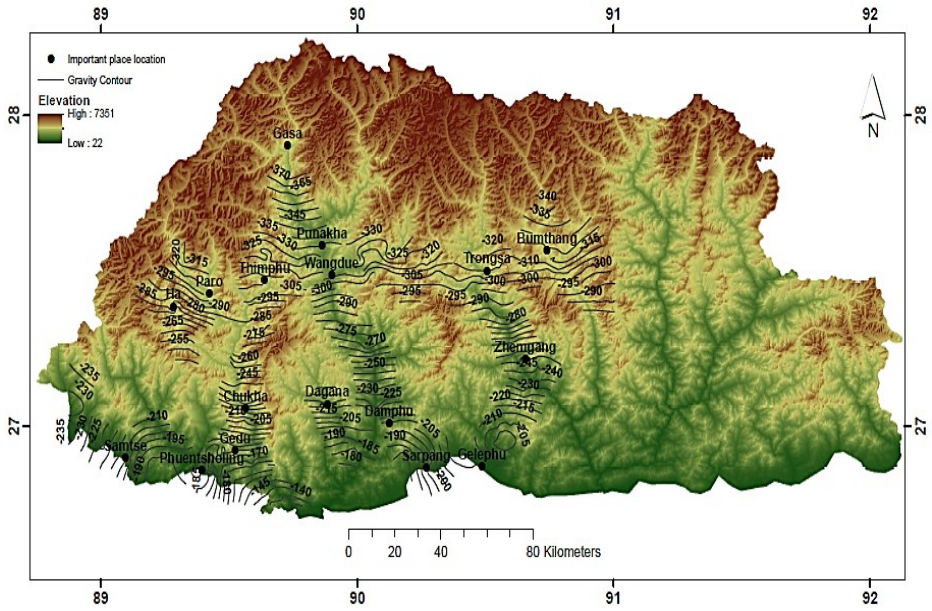

Figure 27. Elevation map of Bhutan overlain with Bouguer gravity anomaly contour. Black lines represent contour lines representing the complete Bouguer gravity anomaly values. As explained in the text, the Bouguer gravity anomaly values are inversely correlated to the elevation values.

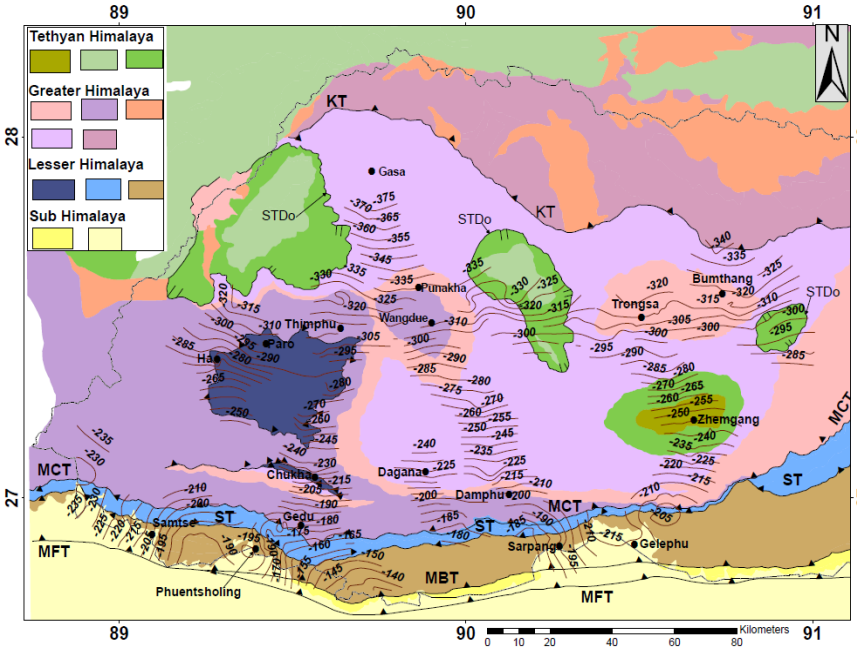

Figure 28. Simplified geologic map of west and central Bhutan (modified after Long et al, 2011c) overlain with the Bouguer gravity anomaly contour. MFT-Main Frontal Thrust, MBT-Main Boundary Thrust, ST-Shumar Thrust, MCT- Main Central Thrust, STDo-Outer South Tibetan Detachment, and KT-Kakhtang Thrust.

5.2 Qualitative Map Analysis Techniques

The Bouguer gravity anomaly map (Fig. 26) reflects the combined effect of density variations occurring at the various depths that cause both local and regional scale gravity anomalies. These variations do not offer any significant insight about boundaries of the distinct geological features or the structures seen on Fig. 28 as the dominant feature of the Bouguer gravity anomaly is a large wavelength anomaly associated with the abrupt thickening of the crust. However, it is possible to extract these broad scale anomalies with the help of various computational methods that are developed for isolating the distinct features of the different sized anomalies. With these methods, we can qualitatively interpret the gravity anomalies in terms of geological features depending of the degree of anomalies arising from it, nevertheless, care must be taken as these numerical manipulations may produce spurious anomalies (Learney and Ulrych, 1986). To enhance the interpretation of the subsurface structures, enhancement techniques such as wavelength filtering that include band-pass and high-pass filtering (Peeples et al., 1986), horizontal and vertical derivatives (Blakely and Simpson, 1986), isostatic gravity residual anomaly (Simpson et al., 1986) and Euler's deconvolution (Reid et al., 1990) were applied to aid in determining the causative sources of these anomalies.

5.2.1 Isostatic Residual Gravity Anomaly Map. Though the Bouguer gravity reduction process removes the gravitational attraction of the topographic masses down to the geoid/mean sea level, any compensating masses that have not been accounted for the Bouguer gravity reduction in mountainous areas manifest themselves as broad Bouguer gravity anomaly lows (Simpson et al., 1986). To retain the residual scale gravity anomalies of geologic interest related to the crust, which are otherwise obscured by the

regional scale topography-induced gravity anomalies caused by the isostatic compensating masses, further isostatic corrections can be made applying the Airy isostasy model (Simpson et al., 1983, 1986). Isostatic gravity anomalies are obtained as the difference between the observed gravity field and the field produced by an isostatically balanced lithosphere.

Topography grids are used to calculate the depth of the compensating material grid below mean sea level by assuming an Airy isostatic model for the regional anomaly calculation at each grid point. The SRTM DEM (90 m spatial resolution) that covers a region 3 degrees surrounding the study which includes the majority of the Himalayan orogenic belt, the southern Tibetan Plateau and northern part of India was used as topography grid. Other parameters to calculate isostatic regional gravity anomalies include thickness of compensating depths, crustal density and Moho density. The crustal thickness in the study varies in between 50 and ~70 km (Singer et al., 2017a). Therefore, several compensating depths ranging between 50 and 70 km were used on trial and error method and it was observed that the results were hugely influenced by the depth values. However, input values of parameters, crustal and Moho density, were found to have less or negligible influence to the regional gravity grid, and hence the resultant isostatic residual gravity anomalies after varying these parameters were observed to differ insignificantly.

To calculate the final isostatic regional gravity grid, a compensating depth of 60 km, crustal density of 2.67g /cm3, and Moho density of 3.3 g /cm3 were used. By subtracting the Bouguer gravity anomaly field from the regional isostatic gravity field, an isostatic residual gravity anomaly map was produced (Fig. 29).

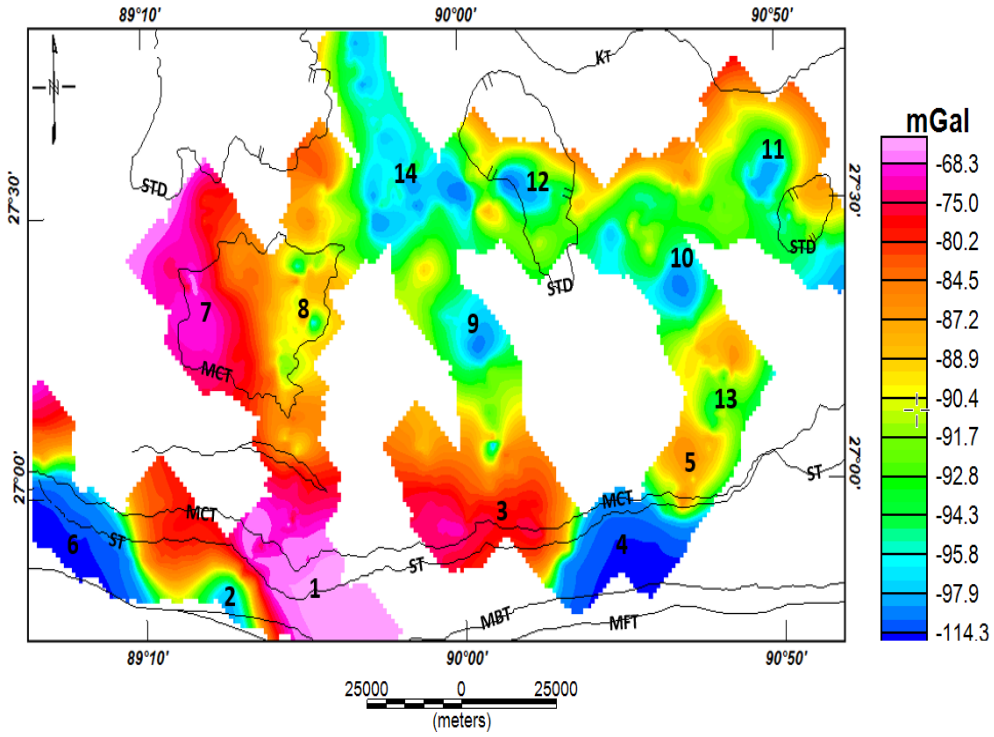

Figure 29. Isostatic residual gravity anomaly map calculated after removing the isostatic regional gravity anomalies from the observed Bouguer anomaly gravity anomalies. A crustal thickness of 60 km, topography density of 2.67 g/cm^3 and Moho density of 3.3 g/cm^3 were used. Numbers on the map refers to gravity anomalies described the text. MFT, MBT, ST, MCT, STD, KT, are same as Figs. 26 and 28.

5.2.2 Band-Pass Wavelength Filtering. By removing the regional gravity effects, a residual gravity anomaly field caused by the lateral density variations, in the near surface/upper crustal structures can be obtained. One method to do this is through wavelength filtering (Peeples et al., 1986). In this method, can remove or enhance anomalies associated with certain wavelengths to isolate features of interest. Band-pass filtering uses a combination of high-pass and lower-pass filters into a single operation to remove both longer and shorter wavelength anomalies. After applying a series of combinations of the wavelengths ranging between 5 and 120 km on a trial and error basis, it was observed that the wavelengths between 10 and 80 km were passed to represent the

residual gravity field that best fits the surface geology of the area. Hence, the residual gravity anomaly map of the complete Bouguer gravity anomaly was prepared using the band-pass filtering technique (Fig. 30).

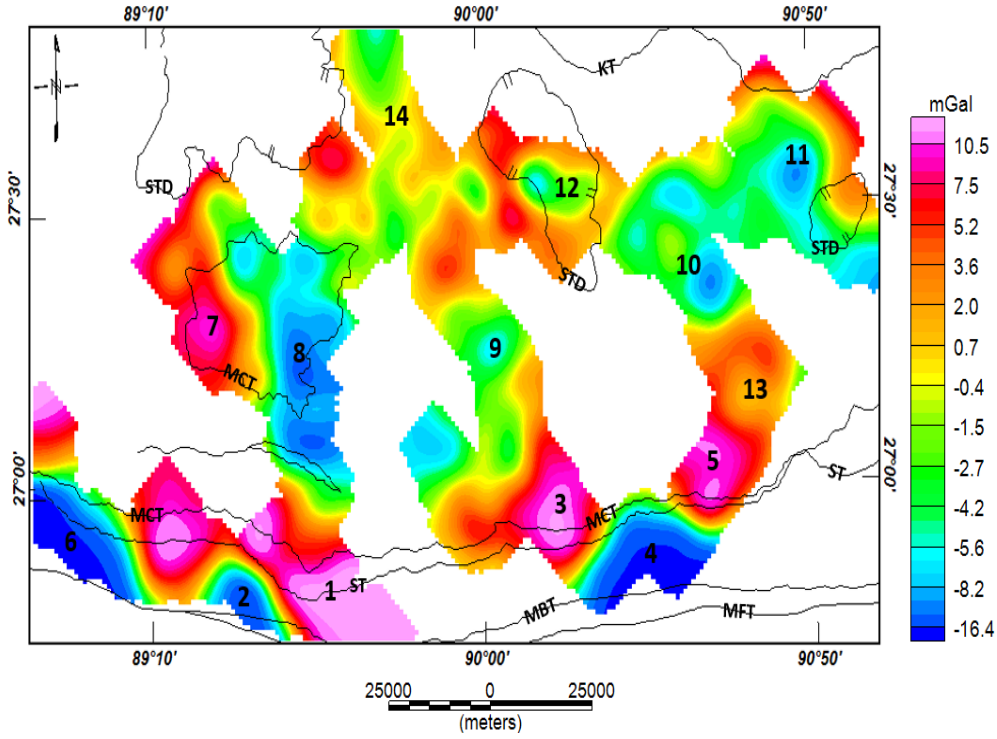

Figure 30. Band-pass filtered residual gravity anomaly map determined by passing wavelengths between 10 and 80 km. Numbers represents the gravity anomalies described in text. MFT, MBT, MCT, ST, STD, and KT are same as Figs. 26 and 28.

5.2.3 Derivative Gravity Anomaly Map. The derivative technique is another useful method for a gravity map analysis which is applied to delineate the edges of subsurface bodies of varying densities (Blakely and Simpson, 1986; Blakely, 1995). Horizontal *x*-derivative and *y*-derivative calculates the rate of change of gravity in the space domain, with respect to *x* and *y* directions. Hence, the horizontal derivatives are the measure of the slope or "gradients" of the anomalies in *x*- and *y* direction, which

generally produces abrupt gradient change approximately over the edge of the density contrast. Vertical derivatives on the other hand, will sharpen the gravity anomalies and are good for determining the width of a density source, and will also emphasize the higher frequency components due to shallow sources relative to the deeper effects. A commonly used edge detection filter is the total horizontal derivative (THDR) formulated by Cordell and Grauch (1986), given by the equation:

$$\text{THDR} = \sqrt{\left(\frac{\partial T}{\partial x}\right)^2 + \left(\frac{\partial T}{\partial y}\right)^2} \qquad (1)$$

where, T is the gravity field, $\partial T / \partial x$ and $\partial T / \partial y$ are the two orthogonal horizontal derivatives of the gravity field. Here, the THDR (Fig. 31) from the *x*-derivative and *y*-derivative using equation (1) and the vertical derivatives (Fig. 32) of the complete Bouguer gravity anomalies were generated.

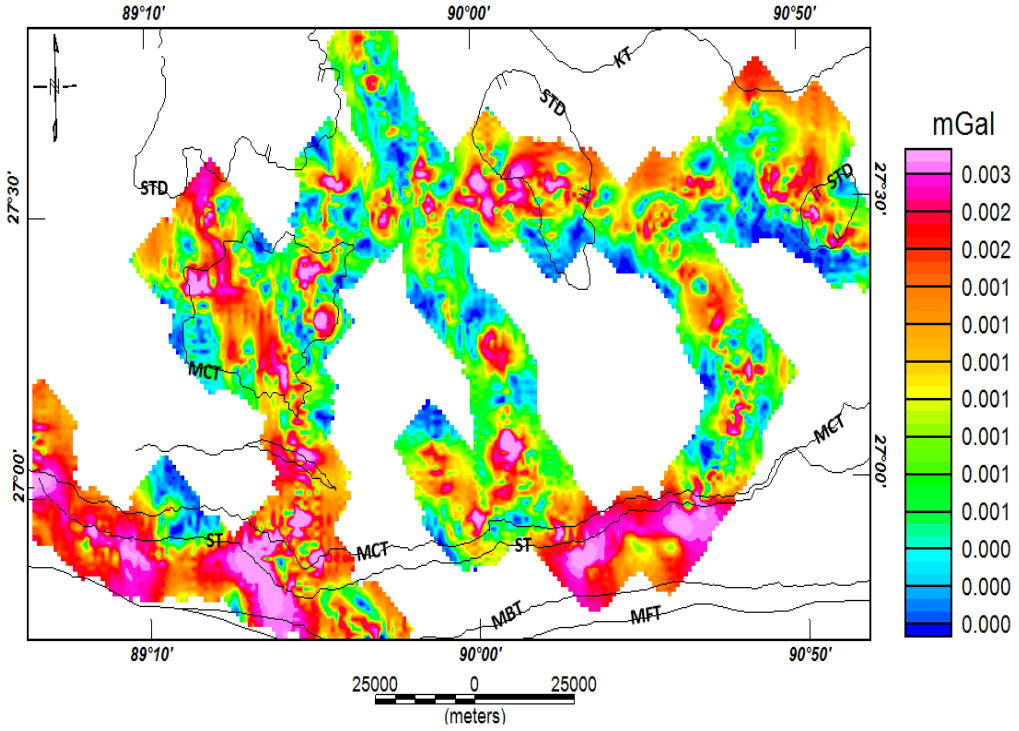

Figure 31. Total horizontal derivative gravity anomaly map of the observed Bouguer gravity anomaly data. MFT, MBT, MCT, ST, STD, and KT are same as Figs. 26 and 28.

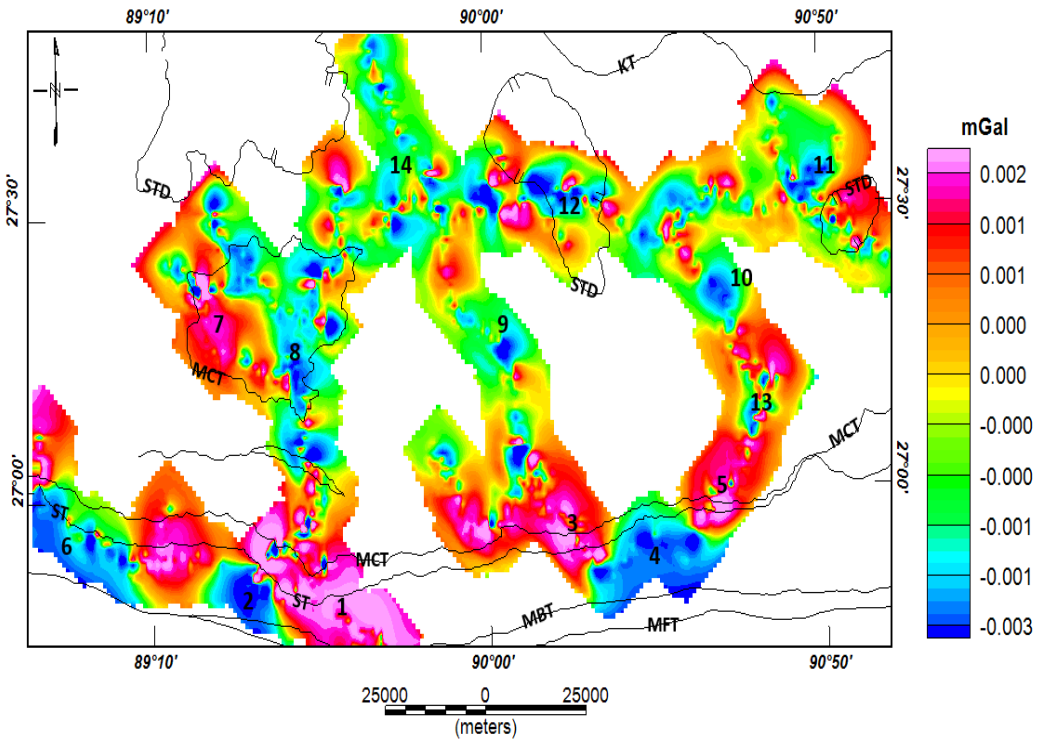

Figure 32. Vertical derivative gravity anomaly map of the observed Bouguer gravity anomaly data. Number in the map refers to gravity anomalies mentioned in text. MFT, MBT, MCT, ST, STD, and KT are same as Figs. 26 and 28.

5.2.4 Euler 3-D Deconvolution Method. Euler deconvolution is used as an interpretation tool to determine the source location of potential field anomalies (Reid et al, 1990; Mushayandebvu et al, 2003; Reid et al, 2014). Euler 3D deconvolution is relatively automated method that provides a 3D interpretation by delineating density boundaries and calculating density source depths using the three orthogonal gradients of the gravity field. This technique is based on the utilization of Euler homogeneity functions theorem introduced by Thomson (1982), which is given by the equation:

$$(x-x_o)\,\delta T/\delta x + (y-y_o)\,\delta T/\delta y + (z-z_o)\,\delta T/\delta z = N\,(B-T) \qquad (2)$$

where, T is the total gravity field, (x_o, y_o, z_o) is the unknown position of a source body or edge to be estimated, and (x, y, z) are the known coordinates of the observation

point of gravity and gradients. The values ($\delta T/\delta x$), ($\delta T/\delta y$) and ($\delta T/\delta z$) are the measured gravity gradients along the x-, y-, and z-directions. B is the regional value of the gravity field to be estimated and N is a non-negative integer commonly known as the structural index (SI) (Reid et al., 1990; Zhang et al., 2000).

With the gravity gradients and suitable SI values shown in Table 3, the variables or unknowns (x_o, y_o, z_o, B) are estimated by using a moving subset or selected windows of a gravity grid. At each window position, a set of linear equations is solved to locate the source in plan and depth (Reid et al., 2014). However, care must be taken while choosing the values of those parameters to achieve results that are geologically meaningful as Reid et al. (2014) explains how to avoid errors by carefully choosing valid parameters.

Table 3. Structural Index values for different structures from Reid et al., 2013

Model	**Magnetic SI**	**Gravity SI**
Points, Sphere	3	2
Line, Cylinder, thin bed fault	2	1
Thin sheet edge, thin sill, think dyke	1	0
Thick sheet edge	0	-1[1]
Contact of infinite depth extent	0	Not useful[2]

[1] Requires the extended definition of SI and a non-linear deconvolution process.
[2] The gravity anomaly is infinite.

To apply the Euler deconvolution algorithm, the Bouguer gravity anomaly data were re-gridded with an interval of 2 km, and both the horizontal and vertical gradients were measured using the Fourier method. Structural Index values of SI=0 and SI=1, and

window size ranging between (3*3 km) and (10*10 km) were investigated. In general, the number of solutions decreased as the window size increased. The solutions for SI=1 do not show a wide range of depth information and the location of the solutions were arbitrary/random, in contrary to the systematic nature of solutions obtained for SI=0. Therefore, an Euler depth solution map (Fig. 33) was constructed using a structural index SI=0, which is to model a thin sheet edge, thin sill, thin dyke, and window size of (3*3 km).

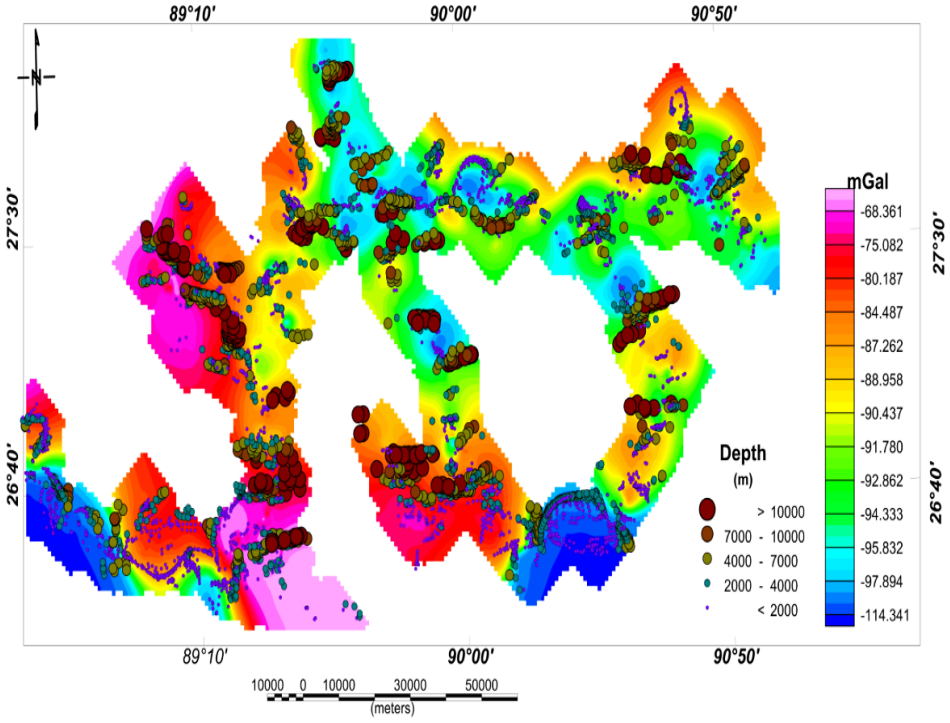

Figure 33. Euler deconvolution solution map superimposed on the isostatic residual gravity anomaly map (Euler solutions were calculated based on the observed gravity gradients, structural index (SI) =0, window size= (3*3 km).

5.3 Gravity Data Interpretation

Substantial deviations from the Bouguer gravity anomaly map (Fig. 26) were observed in the isostatic residual gravity anomaly map (Fig. 29) indicating that there are substantial

anomalies due to crustal density sources and a complex Himalayan geology. A prominent gravity minima, anomaly 2, 4, and 6 (Fig. 29) in the Samtse and Sarpang-Gelephu region is correlated mostly to the Quaternary sediments and sedimentary rocks of the Miocene-Pliocene Siwalik group. These gravity minima can be seen on the residual gravity anomaly map, anomalies 2, 4, and 6 (Fig. 30). However, the width of the anomaly in terms of south-north dimensions, are not in agreement with the nature of outcrops, where the Lesser Himalayan rocks are also presented as gravity minima (anomaly 4). This may be due to the lack of data in this region and this effect is seen in other regions as there are large regions with no data due to the lack of roads.

A gravity maxima can be seen between Gedu and Piping (anomaly 1) and south of the Dagana and Tsiring area (anomaly 2) (Figs. 26, 29, and 30), which is over the Lesser Himalayan sequence. The Paleoproterozoic and Neoproterozoic-Cambrian quarzitic rocks may be the source of this anomaly. Similarly, the western part of Lesser Himalayan rocks exposed in the Paro tectonic window on both the isostatic residual and residual gravity anomaly (Figs. 29, 30) is associated with a gravity maxima (anomaly 7), where the maxima may be due to the high velocities imaged by surface wave ambient noise tomography (Singer et al., 2017a) beneath the Paro Formation. Considerable variation of the size and amplitude of the anomalies is also seen in the residual gravity anomaly maps for most of these regions. Contrary isostatic residual gravity anomalies, the gravity minima (anomaly 8) is seen in the eastern part of Paro window that extends to the Chukha window on the residual gravity anomaly map. This could be related to low density Main Central Thrust zone that bounds the tectonic window from the Greater Himalaya as the anomalies are along or near to this thrust zones. However, there are no

such gravity minima associated with Main Himalayan Thrust or other thrust zones in other locations. In fact, the gravity maxima (anomaly 1, 3 and 5) on both isostatic residual and residual gravity anomaly maps are found along/near-parallel to the Main Central Thrust, suggesting that they resulted from high degree of metamorphism during the thrust motion along the Main Central Thrust.

The Tethyan Himalayan sequence in the Pelala, Zhemgang and Ura regions is associated with a gravity minima (anomalies 10, 11, 12 and 13, Fig. 29) on the isostatic residual gravity anomaly map. Conversely, on the residual gravity anomaly map, a moderate gravity maxima (anomaly 13, Fig. 30) can be seen in the Zhemgang region, which could be related to the quartzite and schist of the Chekha Formation. Gravity minima within the Greater Himalaya (anomalies 9, 10, Figs. 29, 30) are reflected over the Miocene leucogranite units and alternate syncline-anticline folds respectively. Broadly, the density of the rocks increases with an increase in the degree of metamorphism, however, some parts in the Greater Himalayan sequence display an anomaly as low as that produced from Quaternary sediments (anomaly 14, Fig. 29), which needs further investigation.

The THDR gravity map (Fig. 31) is difficult to interpret as only gradient changes were detected mostly along/around the location of the gravity stations, and this could be partly due to the lack of uniformly distributed data and the data are concentrated along roads. Derivative maps work best when there is a uniform coverage of data over a wide region. However, the vertical derivative map shows derivative maxima and minima of a source body (anomalies 1-14, Fig. 32) comparable to that of variation in anomalies detected in the residual gravity anomaly map. Lyon-Caen and Molnar (1985) observed

the gradient of the Bouguer gravity anomaly in the western Himalaya varies from 1mGal/km in the Lesser Himalaya to 2mGal/km in the Greater Himalaya. The increase in the gradient implies that the Moho dips more steeply beneath the Greater Himalayan than beneath the Lesser Himalaya. The Moho geometry in western Bhutan has similar characteristics, for which a comparable gravity gradient was assumed for the study area.

The Euler deconvolution solution map (Fig. 33) shows the depth information of the causative source bodies. Of all categories, the solution that comprises depth information of lesser than 7 km shows systematic clustered points that are connected to the plausible shallow structures, whereas the solution of greater than 7 km are mostly unsystematic. Reid et al. (1990, 2014) described that depths greater than twice the window size are considered unreliable, which could be the cause of this phenomena. Moreover, the gradient maps do not significantly correlates to the probable geologic structures, hence the result in determining the depth information are compromised. Despite these irregularities, solutions from the Euler deconvolution in combination with other gravity maps provided constraints on depth of some anomalies during the gravity modeling.

6. GRAVITY MODELLING AND DISCUSSION

The interpretation of the complete Bouguer gravity anomalies discussed in the previous chapter requires further qualitative analysis to ascertain the location, depth and geometry of the anomaly sources. To quantify the Bouguer gravity anomalies, 2-D gravity forward modeling using GM-SYS in Oasis Montaj^{TM} software along the four transects (Fig. 7) was undertaken to derive plausible density structures and the crustal geometry. The location for transects A-A', B-B', C-C' and D-D' were selected across the Himalayan orogenic wedge such that they cut through all the major geological structures and where the maximum variation in the gravity anomalies were observed. The forward modeling incorporated topography, geological distribution of tectonostratigraphic units (Figs. 7 and 28) and densities of the different rock units.

One of the most common problem encountered in gravity modelling is defining the geometry of the geologic units at depth, as the observed Bouguer gravity anomalies only reveal lateral density variation at depth (Ansari et al., 2014). As a result, existing geologic and geophysical constrains must be used to constrain geologically meaningful models. A few subsurface constraints that available within the study area including seismic studies (Zhao et al., 1993; Hauck et al., 1998; Singer et al., 2017a,b), a regional scale gravity analysis (Hammer et al., 2013), and thermochronologic studies (Coutand et al., 2014). Additionally, there are surface constraints available through geological mapping (Fig. 7). There are no available density data within the study area. Therefore, the near-surface to the upper mantle density values used in gravity modeling in other part of the Himalayan orogeny and listed in Table 4 (Tiwari et al., 2006; Chamoli et al., 2010;

Ansari et al., 2014) were used as initial densities in the models. Additionally, geological balance cross-sections within the area of study (Long et al., 2012, Tobgay et al., 2012; McQuarrie et al., 2014) provided additional constraints on lateral location of different rock units for constructing initial a priori models. The upper crustal structures were further constrained by the isostatic gravity residual and residual gravity from the bandpass filtered maps (Figs. 29 and 30).

The largest subsurface density discontinuity near the surface of the earth occurs at the Moho, the crust-upper mantle boundary, where observed density contrast can delineate subsurface structures (Molnar, 1986; Ansari et al., 2014). Consequently, the geometry and depth the Moho primarily influences the geometries and densities of the upper crustal structures. The initial gravity models were constructed based on: 1) the depth of the Moho inferred from seismic receiver function (RF) analyzes (Hauck et al., 1998; Singer et al., 2017a), and the configuration of another important mid-crustal structure known as the Main Himalayan Thrust from seismic analysis (Singer et al., 2017a) and thermochronologic data (Coutand et al., 2014). 2) The density values of 3.3 g/cc, 2.9 g/cc, 2.78 g/cc were assigned to upper mantle, lower crust, and crustal basement, respectively. For the near-surface rock units, density values of 2.26 g/cc, 2.60 g/cc, 2.66 g/cc, 2.70 g/cc were assigned for the Quaternary sediments, Siwalik Group, Lesser Himalayan units, Greater Himalayan units respectively. 3) The configuration of other major upper crustal tectonic structures including the Main Frontal Thrust, Main Boundary Thrust, Shumar Thrust, Main Central Thrust, and South Tibetan Detachment is based on the balanced cross-sections from the previous studies (Long et al., 2012; Tobgay et al., 2012). For all the above geometries and densities, the list values were

initially used but were varied by up to 10% in order for the calculated anomalies to match the observed Bouguer gravity anomalies.

Table 4. Density values of different rock units used for *a priori* modeling.

Litho-tectonic units	**Density (g/cc)**	**Authors**
Quaternary Sediments	2.26	(Chamoli et al, 2010)
	2.45	(Ansari et al, 2014)
Siwalik Group	2.6	(Chamoli et al, 2010)
	2.55	(Ansari et al, 2014)
Lesser Himalayan	2.52-2.82	(Chamoli et al, 2010)
	2.660	(Ansari et al, 2014)
Greater Himalayan	2.52-2.82	(Chamoli et al, 2010)
	2.70	(Ansari et al, 2014)
Tethyan Himalayan	2.47-2.76	(Chamoli et al, 2010)
	2.650	(Ansari et al, 2014)
Crustal basement	2.78	(Chamoli et al, 2010)
	2.71	(Ansari et al, 2014)
Lower crust	2.9	(Chamoli et al, 2010)
	2.93	(Ansari et al, 2014)
Upper mantle	3.3	(Chamoli et al, 2010)
	3.27	(Ansari et al, 2014)

6.1 Gravity Modeling in Western Bhutan

Two transects A-A’ and B-B’ were modeled in western Bhutan. The first transect (A-A’) is approximately 130 km long extending from Phuentsholing in the south to Gasa, and the second transect (B-B’), which of similar dimension extends from Sarpang to Gasa (Fig. 7). The exact location of transect B-B’ is more of south-central to north-western Bhutan. The crustal thickness along the transects varies from ~50 km to ~70 km, thickening towards north (Singer et al., 2017a) and it has been divided into two main

parts for modeling purposes: Upper crust with crustal basement and the lower crust. Indian basement or crustal basement appellation have been used by various authors (Chamoli et al., 2010; Ansari et al., 2014).

The initial *a priori* models based on the parameters obtained from the previous studies roughly made a good fit between the observed and calculated gravity anomalies. By altering the density values and adjusting the geometries of the crustal interfaces, through an iterative process of a trial and error approach, the subsurface structure beneath western Bhutan Himalaya were imaged in the final models (Figs. 34 and 35). The observed Bouguer gravity values were in agreement with the calculated gravity values by 1 mGal in the final model with the upper crustal density values of different rock units shown in Table 5.

The region of gravity maxima represented anomalies 1 and 3 (Figs. 26, 29, and 30) is supposed to be correlated to the Paleoproterozoic quarzitic rocks of the Shumar Group are modeled with the upper crustal density values of 2.74 g/cc. However, the extension of Shumar Group and Baxa Group (LH in Figs. 34 and 35) were assigned a density value of 2.68 g/cc, which is the initial density derived from the previous studies. At a similar location in the northwest Himalaya, a quartzite metavolcanic body with crustal density values of 2.8 g/cc were modeled beneath the Subhimalaya and Lesser Himalayan sedimentary rocks (Chamoli et al., 2010), but there is no known references for these rocks in the Bhutan Lesser Himalaya due to lack of borehole data in the region. The gravity minima in the south, anomalies 3 and 4 (Figs. 29 and 30) occurs within the Quaternary sediments and sedimentary suites of the Siwalik Group which were provided with crustal density values of 2.26 g/cc and 2.60 g/cc respectively.

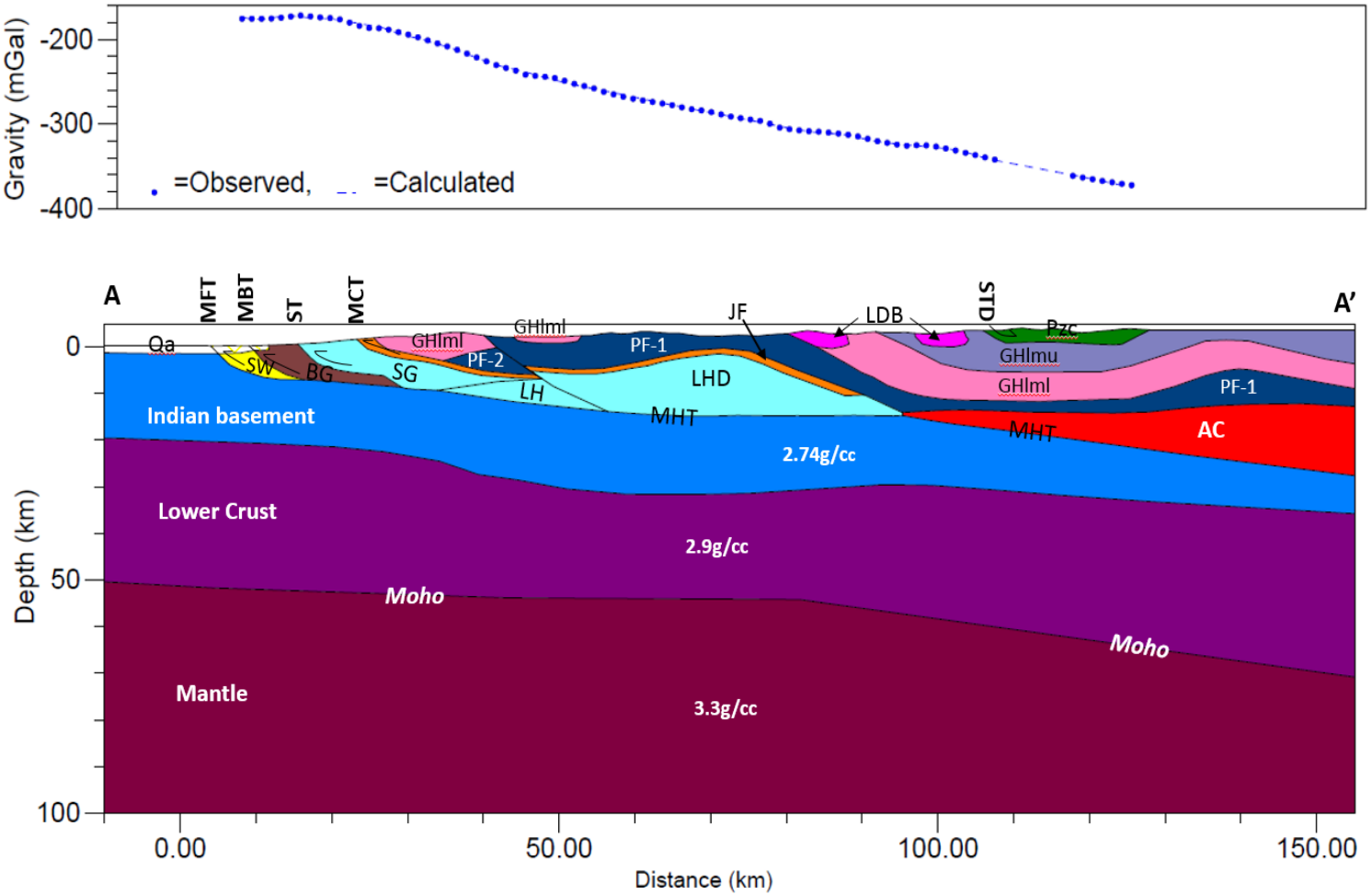

Figure 34. 2-D forward model of the Bouguer gravity anomaly along transect A-A' (Fig. 7). Constrained by the previous geophysical and geological studies listed in the text, observed and calculated Bouguer gravity anomalies variation is less than 2 mGal. MHT-Main Himalayan Thrust, MFT-Main Frontal Thrust, ST-Shumar Thrust, MCT- Main Central Thrust, and STD-South Tibetan Detachment. The density values for the rock units are provided in Table 5.

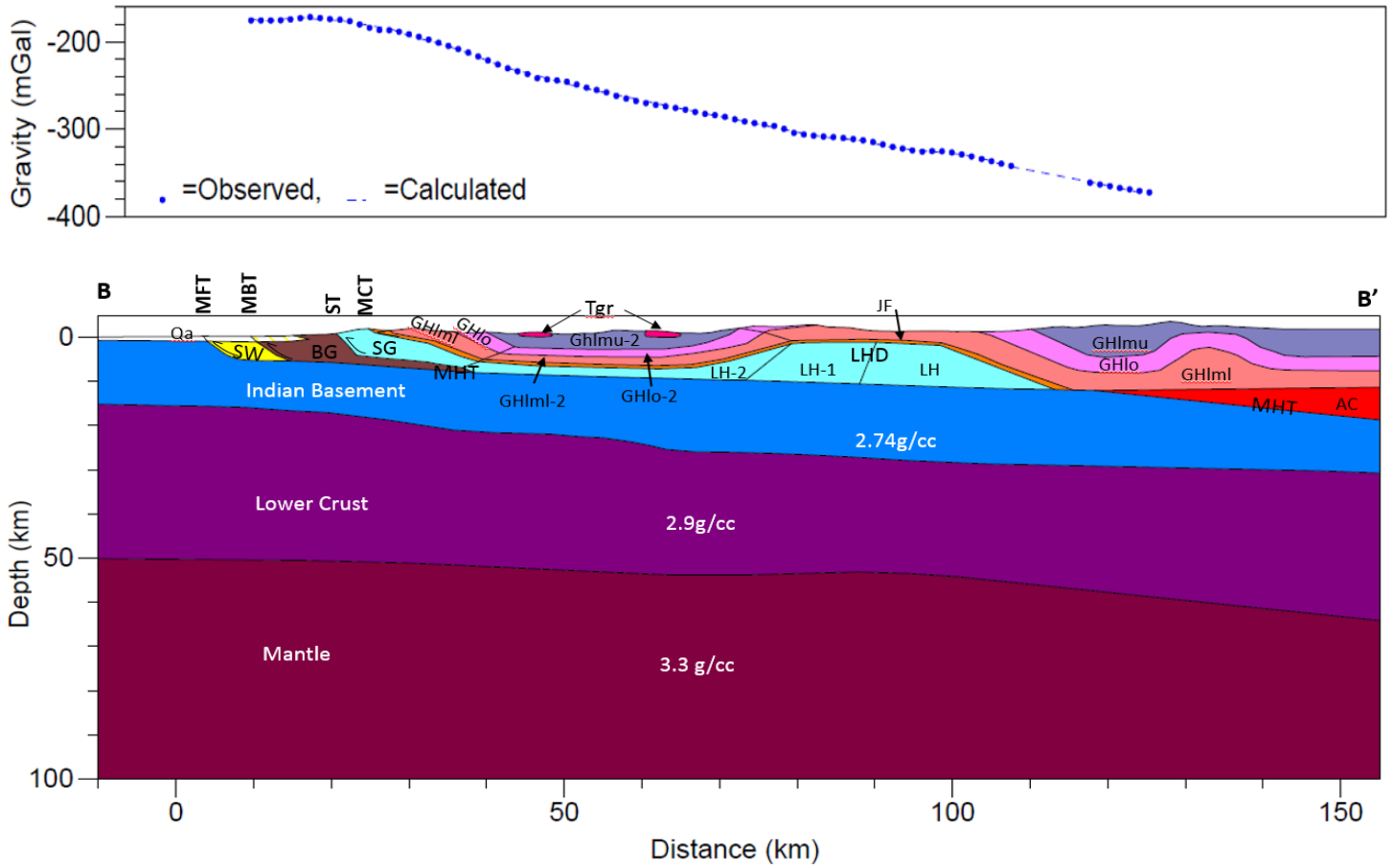

Figure 35. 2-D forward model of the Bouguer gravity anomaly along transect B-B'. Constrained by the previous geophysical and geological studies listed in the text, observed and calculated Bouguer gravity anomalies variation is less than 2 mGal. MHT-Main Himalayan Thrust, MFT-Main Frontal Thrust, ST-Shumar Thrust, MCT- Main Central Thrust, and STD-South Tibetan Detachment. The density values for the rock units are provided in Table 5.

Table 5. Final density values used for modeling in western Bhutan.

Geologic Unit	Sub-unit and Symbol	Density (g/cc)
Quaternary	Qa	2.26
Sub Himalaya	Siwalik Group (SW)	2.60
Lesser Himalaya	Baxa Group (BG)	2.67
	Shumar Group (SG)	2.74
	Lesser Himalaya (LH)	2.68
	Lesser Himalaya (LH-1)	2.72
	Lesser Himalaya (LH-2)	2.65
	Jaishidanda Formation (JF)	2.67
	Paro Formation (PF-1)	2.66
	Paro Formation (PF-2)	2.64
Greater Himalaya	GHlml	2.72
	GHlml-2	2.69
	GHlmu	2.70
	GHlo	2.71
	GHlo-2	2.68
	Low Density Body (LDB)	2.65
	Leucogranite (Tgr)	2.78
Tethyan Himalaya	Chekha Formation (Pzc)	2.66

Along transect A-A' (Fig. 34), the Lesser Himalayan unit is exposed in the Chukha and Paro antiformal tectonic window known as Paro Formation (Tobgay et al., 2010, Singer et al., 2017a,b). The Paro Formation is thrusted over the Lesser Himalayan Duplex by the Paro thrust (Tobgay et al., 2010). The Lesser Himalayan Duplex (LHD) are formed in combination of Baxa and Shumar Group duplex, which accounts for a large fraction of crustal shortening (McQuarrie et al., 2008; Tobgay et al., 2010; Long et al., 2012), were assigned with the upper crustal density values of 2.68 g/cc.

The crustal configuration of the Main Himalayan Thrust and Moho, the crust-mantle boundary, is very much in agreement with the other subsurface models reported in previous studies along the Himalayan orogeny in western Bhutan, Nepal and India (Zhao

et al., 1993; Hauck et al., 1998; Coutand et al., 2014; Singer et al., 2017a). The depth of the Moho increases from ~50 km at the orogenic front to ~70 km beneath the Greater Himalaya, and further increasing towards north. In addition, the Moho dips more steeply beneath the Greater Himalaya than beneath Lesser Himalaya. The abrupt steepening of the Moho occurs at a distance ~65 km towards north from the Himalayan front. This steepening of the Moho has been suggested as a weakening by flexural loading on the Indian plate beneath the Greater Himalayan (Caen-Lyon and Molnar, 1985; Chamoli et al., 2010).

Coutand et al. (2014) determined that the depth of the Main Himalayan Thrust ranges between ~10 and 15 km beneath the Sub and Lesser Himalaya, with the mid crustal ramp along the Main Himalayan Thrust beneath Greater Himalaya through inversion of multithermochronologic data. A similar result was interpreted along transect A-A' from the GANSSER seismic experiment (Singer et al., 2017a) using RF and ambient noise tomography. The gravity models (Figs. 34 and 35) support these interpretations as the Main Himalayan Thrust was located at a depth 6 km beneath the Sub Himalaya, and gradually increasing to ~7-15 km beneath the Lesser Himalaya. The Main Himalayan Thrust beneath the Greater Himalaya are steeper than beneath the Lesser Himalaya, and the depth increases from 15 to ~30 km forming a ramp structure as interpreted by the previous authors. Along this ramp, the crustal basement of Asian crust was modeled as having density values of 2.78 g/cc. This initial value was obtained from a gravity model that crosses the Sikkim Himalaya (Ansari et al., 2014). Most of the Indian and Eurasian plate convergence is assumed to be absorbed along this active basal decollement (Hauck et al, 1998; Singer et al., 2017a). Besides the Moho and Main

Himalayan Thrust, major intra-crustal thrust-fault including Main Central Thrust, Shumar Thrust, Main Boundary Thrust, and Main Frontal Thrust were imaged constructed based on the balanced geological cross-section (McQuarrie et al., 2008; Tobgay et al., 2010). The above thrust faults were observed to be branching out from the Main Himalayan Thrust at a depth varying between 6 and 15 km.

6.2 Gravity Modeling in Central Bhutan

The gravity data acquired in central Bhutan are nonlinear for a long profile. Consequently, two transects, (C-C) and (D-D'), were selected to cover the whole south-north breadth of central Bhutan. Transect C-C' extends from Gelephu to Zhemgang, and transect D-D' continues from Zhemgang to Trongsa (Fig. 7). Aside from the balanced geological cross-sections from Long et al. (2010), there are no geophysical constrains available along these transects. The available geophysical and other subsurface studies were undertaken from western and eastern part of Bhutan, and these studies show significant variation of the crustal structure between these regions. For example, exhumation rates and patterns (Long et al., 2012; McQuarrie et al., 2014; Coutand et al., 2014), decrease in flexural wavelength associated with mantle rheology (Hammer et al., 2014), and structural variation from seismic RF analysis (Singer et al., 2017a,b). These literatures maintaining similar conclusion in west-east structural variations in Bhutan Himalaya provided significant insight in approximating the *a priori* subsurface models along these transects.

The initial models were constructed by assigning the density values for each different rock units identical to those used in the gravity models in western Bhutan

(Figs. 34 and 35). A similar configuration of Moho and the Main Himalayan Thrust used for modeling in western Bhutan was also attempted to fit in the models for central Bhutan. With the Moho geometry similar to the one used for modeling in western Bhutan could not resolve the difference in observed and calculated Bouguer gravity anomalies to an acceptable range in central Bhutan. However, it was observed that the results improved when sub horizontal Moho configuration at depth ~50 km was constructed, which is the depth of Moho suggested in eastern Bhutan through seismic studies (Singer et al., 2017a).

The extent and location of mid-crustal ramp along the Himalayan thrust without seismic constraint was difficult to be detected in the gravity profile. As a consequence, the upper crustal structures including the Main Himalayan Thrust in the a priori models in central Bhutan were established, one as comparable to that of gravity models in western Bhutan and other similar to that of an existing geological cross-section. Subsequently, through a trial and error approach, the error between the observed Bouguer gravity anomalies and the calculated gravity values were reduced from several mGal to less than 1 mGal for all the final gravity models to constraint the crustal structure beneath central Bhutan (Figs. 36, 37 and 38). The final upper crustal density values used for the final models are listed in the Table 6.

The gravity minima, (anomaly 4, Figs. 29 and 30), represents the Quaternary sediment with density values 2.26 g/cc and Miocene-Pliocene Siwalik group with crustal density values 2.6 g/cc. The average thickness of Quaternary sediments in central and western Bhutan is assumed to be 1 km (±.5 km). The interpretation for the residual gravity anomaly maxima (anomaly 5, Fig. 30) in the current models was interpreted same

as that of anomalies 1 and 3 in the western Bhutan models. Both gravity models (Figs. 36 and 37) show a characteristic Himalayan synformal klippe of the Ordovician Chekha Formation and Maneting Formation of the Tethyan Himalaya with varying upper crustal density values of 2.66 g/cc and 2.60 g/cc respectively. However, the Tethyan Himalaya in central Bhutan, within the Zhemgang region, is not separated from the Greater Himalaya by the South Tibetan Detachment system (Long and McQuarrie, 2010; Long et al., 2017). The gravity models also could not image a structure that could describe the South Tibetan Detachment system.

Along the transect D-D', a gravity minima occurs that is represented by anomaly 10 (Figs. 29 and 30). This minima, found between the Tethyan Himalaya and Greater Himalaya orthogenesis units where alternate synclinal-anticlinal structures are being mapped, required reduction in the crustal densities of the Shumar Group, Jashidanda Formation and Orthogneiss unit of Greater Himalaya by up to 3% from the original density values. The depth of this source body was mostly assumed from Euler deconvolution solution map (Fig. 33), but the cause of this remain ambiguous.

From the models (Figs. 34, 35, 36, 37 and 38), significant variations in geometry of the Moho were observed beneath western and central Bhutan. The depth of the Moho runs nearly horizontal at ~50 km along transect C-C', located in the southern part in central Bhutan, which is similar to observations made along the southern part of western Bhutan transects. However, the Moho geometry along transect D-D' that includes the northern part of central Bhutan shows dipping at shallow angle at depth ~50 to 60 km (Fig. 37) in contrast to what was observed beneath Greater Himalayan part of western Bhutan.

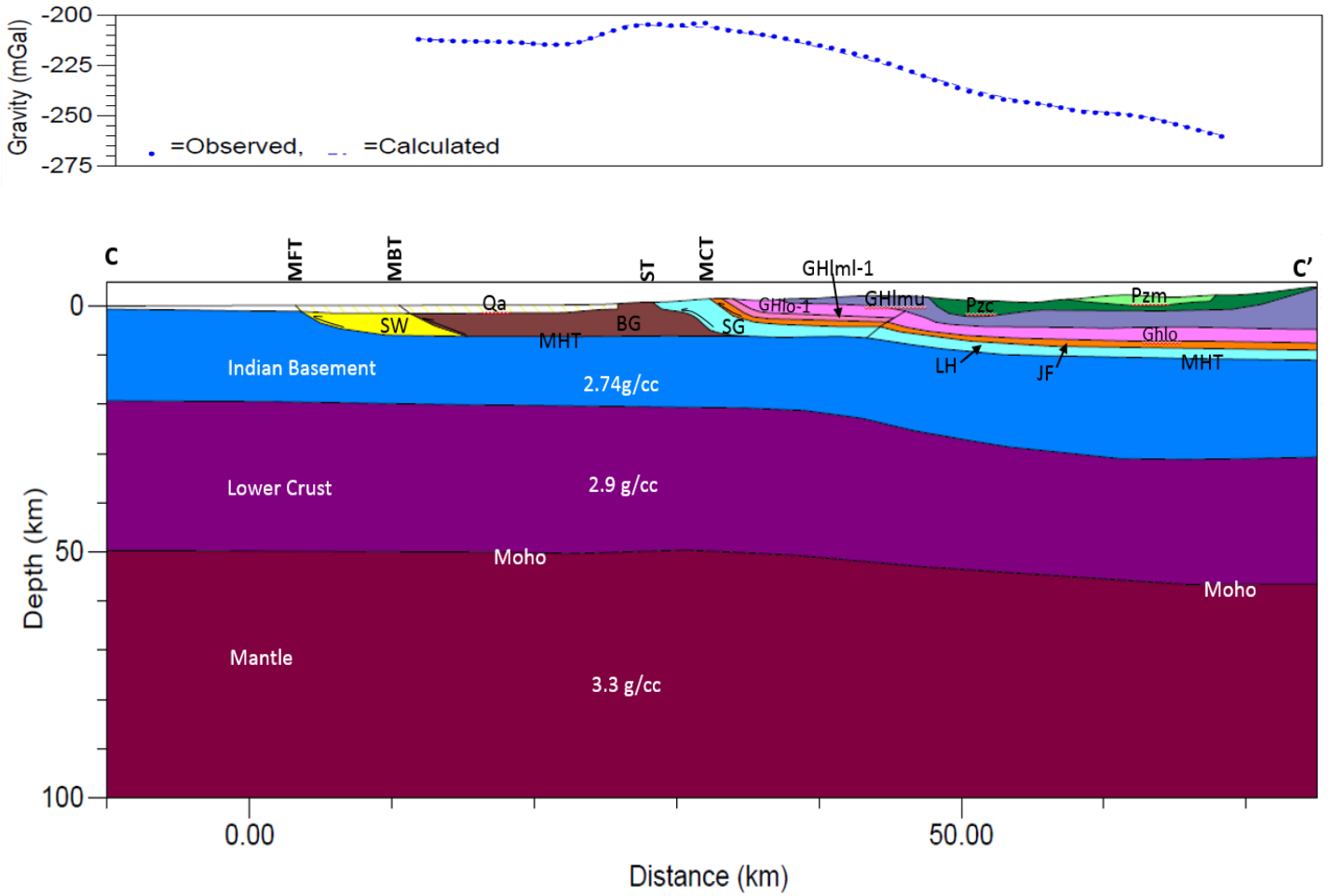

Figure 36. 2-D forward model of the Bouguer gravity anomaly along transect C-C' (Fig. 7). No geophysical constrains are available along this transect. The model was derived from observing the west-east structural variations from previous studies (Coutand et al 2014; Singer et al, 2017a). MHT-Main Himalayan Thrust, MFT-Main Frontal Thrust, ST-Shumar Thrust, and MCT- Main Central Thrust. The density values for the rock units are provided Table 6.

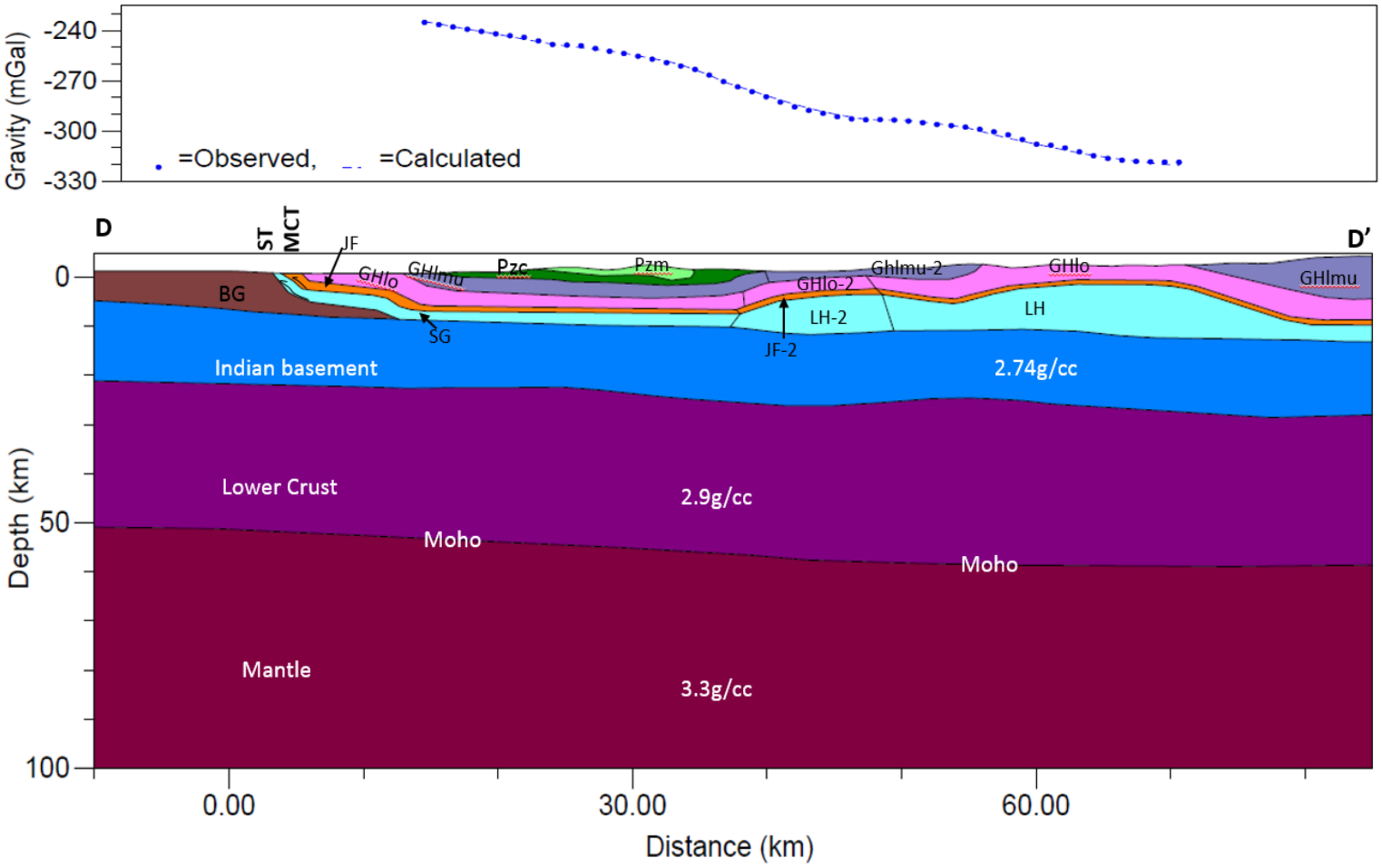

Figure 37. 2-D forward model of the Bouguer gravity anomaly along transect D-D'. No geophysical constrains are available along this transect. The model was derived from observing the west-east structural variations from previous studies (Coutand et al 2014; Singer et al, 2017a). MHT-Main Himalayan Thrust, ST-Shumar Thrust, and MCT- Main Central Thrust. The density values for the rock units are provided Table 6.

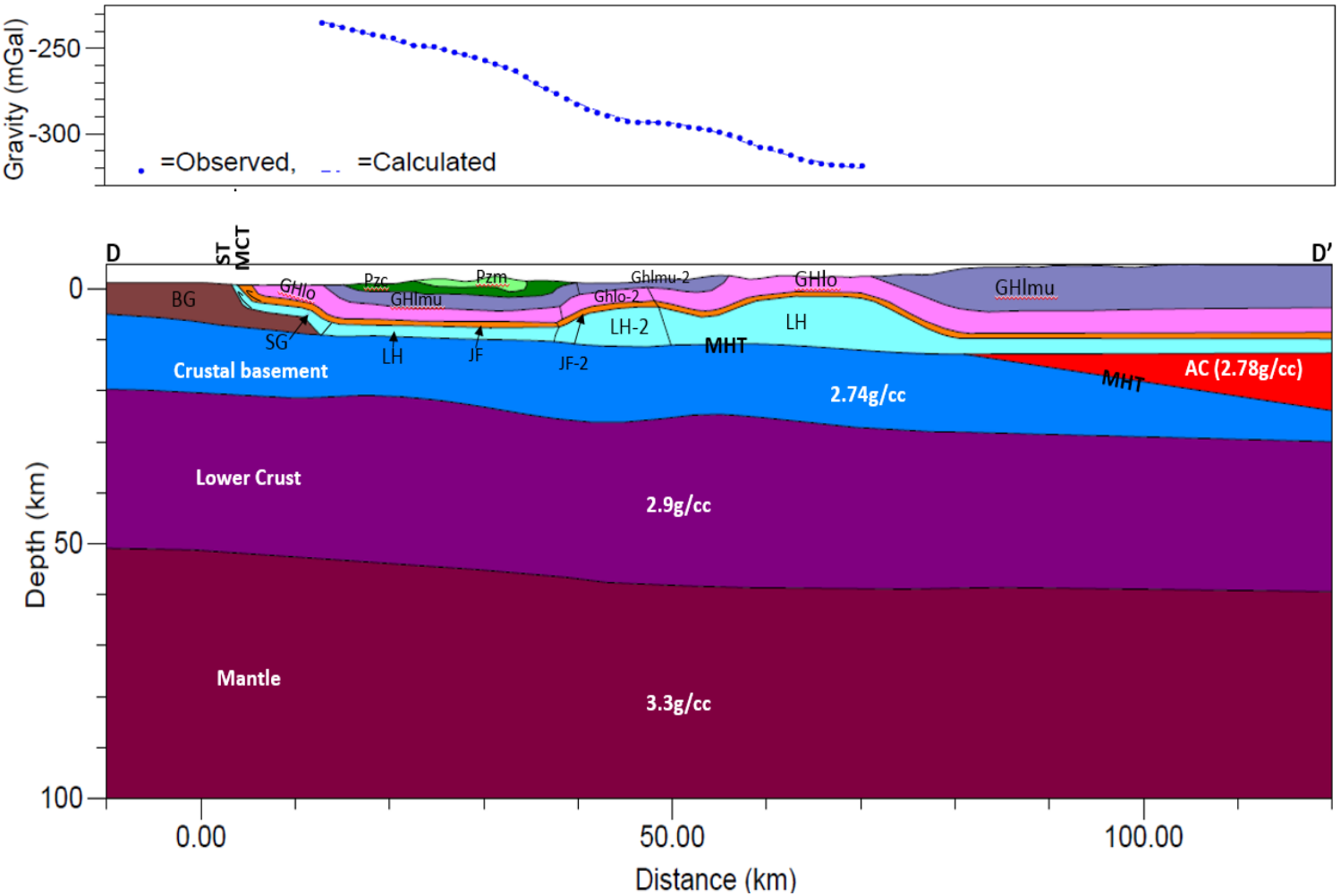

Figure 38. Alternative 2-D forward model of the Bouguer gravity anomaly along transect D-D' (Model-2). The model was constructed to show the mid-crustal ramp along the Main Himalayan Thrust with north extended profile. MHT-Main Himalayan Thrust, ST-Shumar Thrust, and MCT- Main Central Thrust. The density values for the rock units are provided Table 6.

Table 6. Final density values used for modeling in central Bhutan.

Geologic Unit	Sub-unit and Symbol	Density (g/cc)
Quaternary sediments	Qa	2.26
Sub Himalaya	Siwalik Group (SW)	2.60
Lesser Himalaya	Baxa Group (BG)	2.67
	Shumar Group (SG)	2.74
	Lesser Himalaya (LH)	2.68
	Low Himalaya (LH-2)	2.65
	Jaishidanda Formation (JF)	2.67
	Jaishidanda Formation (JF-2)	2.64
Greater Himalaya	GHlml	2.72
	GHlml-1	2.74
	GHlm1-2	2.69
	GHlmu	2.70
	GHlmu-2	2.67
	GHlo	2.71
	GHlo-1	2.73
	GHlo-2	2.68
Tethyan Himalaya	Chekha Formation (Pzc)	2.66
	Maneting Formation (Pzm)	2.60

An alternative models for the Main Himalayan Thrust along transect D-D' (Figs. 37 and 38) were determined to see the effect on the upper and lower crustal density structure by mid-crustal ramp along the Main Himalayan Thrust, and to determine the probable extent of the mid-crustal ramp with the north extended profile. Only a negligible influence was detected, which could be resulted from the absence of gravity anomaly data in the north-central Bhutan as seen in the Fig. 38.

The observed geometry of the Main Himalayan Thrust beneath Sub and Lesser Himalaya (Figs. 36, 37 and 38), varies between 7 and 12 km, is consistent with the

proposed location and depth of the Main Himalayan Thrust in western Bhutan (Figs. 34 and 35). The mid-crustal ramp along the Main Himalayan Thrust beneath the Greater Himalaya, in gravity model (Fig. 38), where depth was estimated from the seismic constraints in western and eastern Bhutan is also found in agreement with the observation made in western Bhutan. Also, no substantial differences in the depth and geometry of the intra-crustal structures, the Main Frontal Thrust, Main Boundary Thrust, Shumar and Main Central Thrust, were detected between the gravity models from western and central Bhutan.

6.3 Discussion

Gravity modeling in the Bhutan Himalaya shows significant structural variations along the west-east strike of the tectonic units within the Himalayan orogeny. The observed geometry of the Moho in western Bhutan is consistent with the result from seismic studies (Singer et al., 2017a), with an abrupt dipping beneath the Greater Himalaya. This northward dipping of the Moho is not observed in eastern Bhutan (Singer et al., 2017a) and central Bhutan in the gravity models from the current study. Singer et al. (2017a) described this difference in the geometry of the Moho in western and eastern Bhutan correlating to the lateral variation of Indian mantle slab with the result from the seismic tomography image (Li et al., 2008).

Li et al. (2008) shows west-east decrease in the extent of Indian mantle lithosphere subducting beneath the southern Tibet with an average depth of 250 km, except at 90°E, 31°N (western Bhutan) where Indian mantle lithosphere is imaged at depths 300-500 km. Singer et al. (2017a) explained that the bending of the Moho in

western Bhutan occurs as the Indian plate in this region is attached with the Indian mantle slab subducting beneath the Lhasa block to the north, which is reaching the maximum depth compared to other location in the Himalayan orogeny. So, western Bhutan is assumed to be the easternmost part of Himalaya influenced by the load exerted by Indian mantle slab on the Indian lithosphere.

The tomographic images between (90° E-95° E) revealed the Indian mantle lithosphere being confined to a shallow depth, and the influence on the Indian lithosphere at this location by Indian slab was not detected, resulting in less pronounced crustal thickening in eastern Bhutan (Li et al., 2008; Singer et al., 2017a). From these discussions, the gravity models from the current study in central Bhutan (between ~ 90.5°E- 91°E) with the subhorizontal Moho geometry (50-60 km) is consistent with the results from tomographic images (Li et al., 2008) and receiver functions analyzes in eastern Bhutan (Singer et al., 2017a). Therefore, based on these arguments and results from the gravity models, it may be assumed that the influence of the Indian mantle slab on the crustal structure in central Bhutan is comparable to that of eastern Bhutan.

Apart from variation of the Moho geometry, the gravity models in western and central Bhutan reveals similar upper crustal density structures including the major tectonic structures. These major thrust faults, the Main Central Thrust, Main Boundary Thrust and Main Frontal Thrust that bounds the tectonostratigraphic units of Himalaya orogeny braches out from the Main Himalayan Thrust at the depth ranging between 7 and 12 km. Although there is no extensive geophysical investigation that provide insight about the structure and depth of these thrust faults, the results from the gravity model is approximately in consistent with the geological cross-sections (Tobgay et al., 2010; Long

et al., 2011). Broadly, the evolution of Himalaya occurred as the crustal shortening of India-Asia convergence starting from early Miocene to the present in Bhutan Himalaya is accommodated along the north to south progression of Himalayan deformation (Long et al., 2012; McQuarrie et al., 2014), which are the major thrust faults described above.

The Himalayan deformation started with the emplacement of Main Central Thrust in early Miocene, Paro and Shumar Thrust ~12-9 Ma, followed deformation along the Main Boundary Thrust and the Main Frontal Thrust during ~9-0 Ma (Long et al., 2012; McQuarrie et al., 2014) . The India-Asia convergence during early and mid-Miocene were accommodated on the Main Central Thrust and the formation of the Paro window duplex and the Lesser Himalayan duplex respectively (Long et al., 2012; McQuarrie et al., 2014). The horizontal shortening rate of the Main Frontal Thrust in Bhutan is estimated to be ~20mm/yr, which is equivalent to the Holocene deformation rate of Himalaya (Berthet et al., 2014).

7. CONCLUSIONS

The gravity field from newly acquired detailed gravity data in western and central Bhutan has been primarily interpreted to reflect the Cenozoic to present day tectonic evolution of Himalayan orogeny caused by the collision and convergence between Indian plate and Eurasian plate. These data provide the first potential field constraints on the lithospheric structure within the Bhutan Himalaya. The combination of map method analysis (wavelength filtering) and 2-D gravity models reveals insight on the geometries and extends of lithospheric structures across the study area. The Bhutan Himalaya is characterized by a prominent Bouguer gravity anomaly low, similar to other locations in the orogenic belt, with south-north trending gradient caused by the thickening of the crust from south towards north. Residual gravity anomaly maps reflecting crustal density changes constructed using isostatic residual gravity and band-pass filtering techniques reflect a series of gravity minima and maxima mostly associated with Miocene Siwalik Group, Quaternary sediments and Paleoproterozoic lesser Himalayan units. No substantial causative source bodies are evident from the derivatives gravity anomaly maps and thus interpreting 3-D Euler Deconvolution results are ambiguous and needs further investigation.

Four approximately north-south trending gravity models across the main tectonic units are constrained by geologic mapping, seismic and regional gravity studies. The models illustrate the high-resolution subsurface structures within the study area and show significant changes in crustal thickness between western and central Bhutan that may reflect the influence of activity or motion of Indian mantle-slab subducting beneath the

Lhasa block similar to that of western and eastern Bhutan (Singer et al., 2017a). In western Bhutan, the depth of Moho increases from 50 km in the south to 70 km in the north with abrupt bending beneath the Greater Himalaya. In contrary, the Moho depth in central Bhutan varies between 50 km in the south to ~60 km in the north without a noticeable abrupt bending.

However, there are no significant variations in the upper-crustal structures were detected. The Main Himalayan Thrust varies between 7 and 30 km with the formation mid-crustal ramp structure along the thrust beneath the Greater Himalaya in western Bhutan, of which similar configuration is determined in the central Bhutan. The gravity models also determined the plausible location and depth of other major tectonic structures including the Main Frontal Thrust, Main Boundary Thrust, Shumar Thrust, Main Central Thrust and South Tibetan Detachment system.

REFERENCES

Acton, C. E., Priestly, K., Mitra, S., and Gaur V. K., 2011, Crustal structure of the Darjeeling-Sikkim Himalaya and southern Tibet: Geophysical Journal International, v. 184, p. 829-852.

Adam, B. A., Whipple, K. X., Hodges, K. V., and Hiemsath, A. M., 2016, In situ development of high elevation, low-relief landscapes via duplex formation in the Himalayan hinterland, Bhutan: Journal of Geophysical Research Earth Surface, v. 121, p. 294-319.

Ansari, M. A., Khan, P. K., Tiwari, and V. M., Banerjee, J., 2014, Gravity anomalies, flexure, and deformation of the converging Indian lithosphere in Nepal and Sikkim-Darjeeling Himalayas: International Journal of Earth Science, v. 103, p. 1681-1697.

Avouac, J. P., 2003, Mountain building, erosion, and the seismic cycle in the Nepal Himalaya: Advances in Geophysics, v. 46, p. 1-80.

Avouac, J. P., 2007, Dynamic processes in extensional and compressional settings-Mountain Building: From earthquakes to geological deformation: Treatise Geophysics, p. 377-439.

Bai, Z., Zhang, S., and Braitenberg, C., 2013, Crustal density structure from 3D gravity modelling beneath Himalaya and Lhasa blocks, Tibet: Journal of Asian Earth Sciences, v. 78, p. 301-317.

Beaumont C., Jamieson R. A., Nguyen, M. H., and Lee, B., 2001, Himalayan tectonics explained by extrusion of a low-viscosity crustal channel coupled to focused surface denudation: Nature, v. 414, p. 738-742

Beaumont C., Jamieson R. A., Nguyen, M. H., and Lee, B., 2004, Crustal channel flows: 1. Numerical models with application to the tectonics of the Himalayan-Tibetan orogeny: Journal of Geophysical Research Solid Earth, v. 109, B06406.

Blakely, R. J., 1995, Potential Theory in Gravity & Magnetic Applications: Cambridge University Press, New York.

Blakely, R. J., and Simpson, R. W., 1986, Approximating edges of the source bodies from magnetic or gravity anomalies: Geophysics, v. 51, p. 1494-1498.

Carrapa, B., Robert, X., DeCelles, P. G., Orme, D. A, Thomson, S. N, and Schoenbohm, L. M., 2016, Asymmetric exhumation of the Mount Everest region: Implications for the tectono-topographic evolution of the Himalaya: Geological Society of America Bulletin, v. 44, p. 611-614.

Chamoli, A., Pandey, A. K., Dimri, V. P., and Banerjee, P., 2010, Crustal configuration of the Northwest Himalaya based of modelling of gravity data: Pure and Applied Geophysics, doi: 10.1007/s00024-010-0149-2.

Cordell, L., and Grauch, T., 1987. Limitations of determining density or magnetic boundaries from the horizontal gradient of gravity or pseudogravity data: Geophysics, v. 52, p. 118-121.

Coutand, I., Barrier, L., Govin, G., Grujic, D., Hoorn, C., Dupont-Nivet, G. and Najman, Y., 2016, Late Miocene-Pleistocene evolution of India-Eurasia convergence partitioning between the Bhutan Himalaya and the Shillong Plateau: New evidences from foreland basin deposits along the Dungsam Chu section, eastern Bhutan: Tectonics, v. 35, p. 2963–2994,

Coutand, I., Whipp Jr., D. M., Grujic, D., Bernet, M., Fellin, M. G., Bookhagen, B. B., Landry, K. R., Ghalley, S. K., and Duncan, C., 2014, Geometry and kinematics of the Main Himalayan Thrust and Neogene crustal exhumation in the Bhutanese Himalaya derived from inversion of multithermochronologic data: Journal of Geophysical Research Solid Earth, v. 119, p. 1-36.

Davidson, C., Grujic, D. E., Hollister, L. S., and Schmid, S.M., 1997, Metamorphic reactions related to decompression and synkinematic intrusion of leucogranite, High Himalayan crystallines, Bhutan: Journal of Metamorphic Geology, v. 15, p. 593–612.

DeCelles, P. G., Geherels, G. E., Quade, J., LaReau, B., and Spurlin, M., 2000, Tectonic implications of U-Pb zircon ages of the Himalayan orogenic belt in Nepal: Science, v. 288, p. 497-499.

DeCelles, P. G., Geherels, G. E., Quade, J., and Ojha, T. P., 1998, Eocene early Miocene foreland basin development and the history of Himalayan thrusting, western and central Nepal: Tectonics, v. 17, p. 741-765.

Dietrich, V., and Gansser, A., 1981, The leucogranites of the Bhutan Himalaya (crustal anatexis versus mantle melting): Schweizerische Mineralogische und Petrographische Mitteilungen, v. 61, p. 177–202.

Gansser, A., 1964, Geology of the Himalaya: Wiley- Interscience, New York, 289 p.

Gansser, A., 1983, Geology of the Bhutan Himalaya: Birkhauser Verlag, Boston, 181 p.

Gehrels, G. E., DeCelles, P., Martin, A. J., Ojha, T., Pinhassi, G., and Upreti, B. N, 2003, Initiation of the Himalayan Orogen as an early Paleozoic thin-skinned thrust belts: Geological Society of America Today, v. 13, p. 4-9.

Godin, L., Grujic, D., Law, R. D., and Searle, M. P., 2006, Channel flow, ductile extrusion and exhumation in continental collision zones: An introduction: Geological Society, London, Special Publications, v. 268, p. 1-23.

Greenwood, L. V., Argles, T. W., Parrish, R.R., Harris, N. B. W., and Warren, C., 2015, The geology and tectonics of central Bhutan: Journal of the Geological Society, doi:10.1144/jgs2015-031.

Grujic, D., Casey, C., Davidson, C., Hollister, L. S., Kundig, R., Pavlis, T., and Schmid, S., 1996, Ductile extrusion of the Higher Himalayan Crystalline in Bhutan: Evidence from quartz microfabrics: Tectonophysics, v. 260, p. 21-43.

Grujic, D., Hollister, L. S., and Parrish, R. R., 2002, Himalayan metamorphic sequence as an orogenic channel: Insight from Bhutan: Earth and Planetary Science Letters, v. 198, v. 177-191.

Hammer, P., Berthet, T., Hetenyi, G., Cattin, R, Drukpa, D., Chophel, J., Lechmann, S., Moigne, N.L., Champollion, C., and Doerflinger, E., 2013, Flexure of the India plate underneath the Bhutan Himalaya: Geophysical Research Letters, v. 40, p. 4225-4230.

Hauck, M. L., Nelson, K. D., Brown, L. D., Zhao, W., and Ross, A. R., 1998, Crustal structure of the Himalayan orogeny at ~90° east longitude from Project INDEPTH deep reflection profiles: Tectonics, v. 17, p. 481-500.

Heim, A. and Gansser, A., 1939, Central Himalaya-Geological observations of the Swiss expedition, 1936: Zürich, Mémoires de la Société Helvétique des Naturelles, v. 73, 245 p.

Hodges, K. V., 2000, Tectonics of the Himalaya and southern Tibet from two perspectives: Geological Society of America Bulletin, v. 112, p. 324-350.

Hollister, L. S., and Grujic, D., 2006, Pulsed channel flow in Bhutan, in Channel Flow, Ductile Extrusion and Exhumation in Continental Collision Zones: Geological Society of London, Special Publication, v. 268, p. 415–423.

Hughes, N. C., Myrow, P. M., McKenzie, N. R., Harper, D. A. T., Bhargava, O. N., Tangri, S. K., Ghalley, K. S., and Fanning C. M., 2010, Cambrian rocks and faunas of the Wachi La, Black Mountains, Bhutan: Geological Magazine, doi:10.1017/S0016756810000750.

Kellett, D.A., Grujic, D., and Erdmann, S., 2009, Miocene structural reorganization of the South Tibetan detachment, eastern Himalaya: Implications for continental collision: Lithosphere, v. 1, p. 259-281.

Le Fort, P., 1975, Himalayas: The collided range, present knowledge of the continental arc: American Journal of Science, v. 275-A, p. 1-44.

Learney, S. W., and Ulrych, T. J., 1986, Multiple dynamic matching: A new approach to well log correlation: Geoexploration, v. 24, p. 503-515.

Li, C., van der Hilst, R. D., Meltzer, A. S., and Engdahl, E. R., 2008, Subduction of the Indian lithosphere beneath the Tibetan Plateau and Burma: Earth and Planetary Science Letters, v. 274, p. 157-168.

Long, S., and McQuarrie, N., 2010, Placing limits on channel flow: Insights from the Bhutan Himalaya: Earth and Planetary Science Letters, v. 290, p. 375-390.

Long, S., Gordon, S. M., and Soignard, E., 2017, Distributed north-vergent shear and flattening through Greater and Tethyan Himalayan rocks: Insights from metamorphic and strain data from the Dangchu region, central Bhutan: Lithosphere, v. 9, p. 774-795.

Long, S., McQuarrie, N., Tobgay, T., Coutand, I., Cooper, F., Reiners, P., Wartho, J., and Hodges, K. V., 2012, Variable shortening rates in the eastern Himalayan thrust belt, Bhutan: Insight from multiple thermochronologic and geochronologic datasets tied to kinematic reconstructions: Tectonics, v. 31, TC5004, doi:10.1029/2012TC003155.

Long, S., McQuarrie, N., Tobgay, T., Rose, C., Gehrels, G., and Grujic, D., 2011a, Tectonostratigraphy of the Lesser Himalaya of Bhutan: Implications for the along -strike stratigraphic continuity of the northern Indian margin: Geological Society of America Bulletin, v. 123, p. 1406-1426.

Long, S., McQuarrie, N., Tobgay, T., and Grujic, D., 2011b, Geometry and Crustal shortening of the Himalayan fold-thrust belt, eastern and central Bhutan: Geological society of America Bulletin, v. 123 (7-8), p. 1427-1447.

Long, S., McQuarrie, N., Tobgay, T., Grujic, D., and Hollister, L., 2011c, Geologic map of Bhutan: The Journal of Maps, v. 2011, p. 184-192.

Lyon-Caen, H., and Molnar, P., 1985, Gravity anomalies, flexure of the Indian Plate, and the structure, support and evolution of the Himalayan and Ganga Basin: Tectonics, v. 4, p. 513-538.

Martin, A. J., 2017, A review of Himalayan stratigraphy, magmatism, and structure: Gondwana Research, v. 49, p. 42-80.

Martin, A. J., DeCelles, P. G., Gehrels, G. E., Patchett, P. J., and Isachen, C., 2005, Isotopic and structural constraints on the location of the Main Central thrust in the Annapurna Range, central Nepal Himalaya: Geological Society of America Bulletin, v. 117, p. 926-944.

McQuarrie, N., Robinson, D., Long, S., Tobgay, T., Grujic, D., Geherals, G., and Ducea, M., 2008, Preliminary stratigraphic and structural architecture of the Himalayan system: Earth and Planetary Science Letters, v. 272, p. 105-117.

McQuarrie, N., Tobgay, T., Long, S. P., Reiners, P. W., and Cosca, M. A., 2014, Variable exhumation rates and variable displacement rates: Documenting recent slowing of Himalayan shortening in western Bhutan: Earth and Planetary Science Letters, v. 386, p. 161-174.

Molnar, P., 1986, The Geologic History and Structure of the Himalaya: American Scientist, v. 74, p. 144-154.

Morelli, C., 1976, Gravimetry, general report: International Geodesy, v. 25, p. 94-113.

Mushayandebvu, M. F., Lesur, V., Reid, A. B., and Fairhead, J. D., 2004, Grid Euler deconvolution with constraints for 2D structures: Geophysics, v. 69, p. 489-496.

Myrow, P. M., Hughes, N. C., Paulsen, T. S., Williams, I. S., Parcha, S. K., Thomson, K. R., Bowring, S. A., Peng, S. C., and Ahluwalia, A. D., 2003, Integrated tectonostratigraphic analysis of the Himalaya and implications for its tectonic reconstruction: Earth and Planetary Science Letters, v. 212, p. 433-441.

Nábělek, J., Hetényi, G., Vergne, J., Sapkota, S., Kafle, B., Jiang, M., Su, H., Chen, J., Huang, B. S., and the Hi-CLIMB Team, 2009, Underplating in the Himalaya-Tibet Collision zone revealed by Hi-CLIMB experiment: Science, v. 325, p. 1371-1374.

Parrish, R., and Hodges, K., 1996, Isotopic constraints on the age and provenance of the Lesser and Greater Himalayan sequence, Nepalese Himalaya: Geological Society of America Bulletin, v. 108, p. 904-911.

Peeples, W. J., Coultrip, R. L., and Keller, G. R., 1986, Quasi-ideal spatial filters for large maps: Anuale Geophysicae, v. 4, p. 547-554.

Quade, J., Cater, J. M. L., Ojha, T., Adam, J., and Harrison, T. M., 1995, Late Miocene environmental change in Nepal and northern Indian subcontinent: Stable isotopic evidence from Paleosols: Geological Society of America Bulletin, v. 107, p. 1381-1397.

Reid A. B., Allsop, J. M., Granser, H., Melletts, and Somerton I. W., 1990, Magnetic interpretation in three dimensions using Euler deconvolution: Geophysics, v. 55, p. 80-91.

Reid, A. B., Jörg, E., and Webb, S. J., 2014, Avoidable Euler Errors- the use and abuse of Euler deconvolution applied to potential fields: Geophysical Prospecting, p. 1-7.

Searle, M., 2013, Colliding continents: A geological exploration of the Himalaya, Karakoram, and Tibet: Oxford University Press, 438 p.

Simpson, R. W., Saltus, R. W., Jachens, R. C., and Godson, R. H., 1983, A description of colored isostatic gravity maps and a topographic map of the Conterminous United States: United State Geological Survey Open-File Report 83-884.

Simpson, R. W., Jachens, R. C., and Blakely R. J., 1986, A new isostatic residual gravity map of the Conterminous United States with a discussion on the significance of isostatic residual anomalies: Journal of Geophysical Research Solid Earth, v. 91, p. 8348-8372.

Singer, J., Kissling, E., Diehl, T., and Hetényi, G., 2017a, The underthrusting Indian crust and its role in collision dyanamics of the Eastern Himalaya in Bhutan: Insight from receiver function imaging: Journal of Geophysical Research Solid Earth, v. 122, doi: 10.1002/2016JB013337.

Singer, J., Obermann, A., Kissling, E., Fang, H., Hetényi, G., and Grujic, D., 2017b, Along-strike variations in the Himalayan orogenic wedge structure in Bhutan from ambient seismic noise tomography: Geochemistry, Geophysics, Geosystem, v. 18, p. 1483-1498.

Sorkhabi, R., 2010, Geologic formation of Himalaya: The Himalayan Journal, v. 66.

Swapp, S. M., and Hollister, L. S., 1991, Inverted metamorphism within the Tibetan slab of Bhutan: Evidence for a tectonically transported heat source: Canadian Mineralogist, v. 29, p. 1019–1041.

Takada, Y, and Matsu'ura, M., 2007, Geometric evolution of plate interface-branch fault system: Its effects on the tectonic development of the Himalayas: Journal of Asian Earth Sciences, v. 29, p. 490-503.

Tangri, S. K., and A. C. Pande, 1995, Tethyan sequence, in The Bhutan Himalaya: A Geological Account, O. N. Bhargava (ed.): Special Publication Service, Geological Survey of India, v. 39, p. 109–141.

Thomson, D., 1982. Euldph: A new technique for making computer assisted depth estimates from magnetic data: Geophysics, v. 47, p. 31-37.

Tobgay, T., Long, S., McQuarrie, N., Ducea, M. N. and Gehrels, G., 2010, Using isotopic and chronologic data to fingerprint strata: Challenges and benefits of variable sources to tectonic interpretations, the Paro Formation, Bhutan Himalaya: Tectonics, v. 29, TC6023, doi: 10.1029/2009TC002637.

Tobgay, T., McQuarrie, N., Long S., Kohn M. J. and Corrie, S. L., 2012, The age and rate of displacement along the Main Central Thrust in the western Bhutan Himalaya: Earth and Planetary Science Letters, p. 146-158.

Upreti, B. N., 1999, An overview of the stratigraphy and tectonics of the Nepal Himalaya: Journal of Asian Earth Science, v. 17, p. 577-606.

Wang, E., Kamp P. J. J., Xu, G., Hodges, K. V., Meng, K., Chen, L., Wang, G., and Luo, H., 2015, Flexural bending of southern Tibet in a retro foreland setting: Scientific Reports, doi: 10.1038/srep12076.

Webb, A. A. G., Guo, H., Clift, P. D., Husson, L., Muller, T., Costantino, D., Yin, A., Xu, Z., Cao, H., and Wang, Q., 2017, The Himalaya in 3D: Slab dyanamics controlled mountain building and monsoon intensification: Lithosphere, v. 9, p. 637-651.

Wittlinger, G., Farra, V., Hetényi, G., Vergne, J., and Nábělek, J., 2009, Seismic velocities in Southern Tibet lower crust: a receiver function approach for eclogite detection: Geophysical Journal of International, v. 177, p. 1037-1049.

Yin, A., 2006, Cenozoic tectonic evolution of the Himalayan orogen as constrained by along-strike variation of structural geometry, exhumation history, and foreland sedimentation: Earth Sciences Review. 76, p. 1-131.

Zhao, W., Nelson, K. D., and Project INDEPTH Team, 1993, Deep seismic reflection evidence for continental underthrusting beneath southern Tibet: Nature, v. 366, p. 557-559.

Zhang, C., Mushayandebvu, M. F., Reid, A. B., Fairhead, J. D. and Odegard, M. E., 2000, Euler deconvolution of tensor gradient gravity data: Geophysics, v. 65, p. 512–520.